3-1-2018

Utilizing Supercomputing to Analyze Risks of an Emergent Large-Scale Debris Field in Low Earth Orbit

David J. Buehler

UTILIZING SUPERCOMPUTING TO ANALYZE RISKS OF AN EMERGENT LARGE-SCALE DEBRIS FIELD IN LOW EARTH ORBIT

THESIS

David J. Buehler, Second Lieutenant, USAF
AFIT-ENV-MS-18-M-184

DEPARTMENT OF THE AIR FORCE
AIR UNIVERSITY

AIR FORCE INSTITUTE OF TECHNOLOGY

Wright-Patterson Air Force Base, Ohio

AFIT-ENV-MS-18-M-184

UTILIZING SUPERCOMPUTING TO ANALYZE RISKS OF AN EMERGENT LARGE-SCALE DEBRIS FIELD IN LOW EARTH ORBIT

Presented to the Faculty

Department of Systems Engineering and Management

Graduate School of Engineering and Management

Air Force Institute of Technology

Air University

Air Education and Training Command

In Partial Fulfillment of the Requirements for the

Degree of Master of Science in Systems Engineering

David J. Buehler, B.S. Chemical Engineering

Second Lieutenant, USAF

March 2018

AFIT-ENV-MS-18-M-184

UTILIZING SUPERCOMPUTING TO ANALYZE RISKS OF AN EMERGENT LARGE-SCALE DEBRIS FIELD IN LOW EARTH ORBIT

David J. Buehler, B.S. Chemical Engineering

Second Lieutenant, USAF

Committee Membership:

Colonel Dane Fuller
Chairman

Dr. John Colombi
Member

Dr. William Wiesel
Member

Mr. David Meyer
Member

Abstract

The likelihood of on-orbit breakups, whether spontaneous or the result of collision, will likely continue to grow as the barriers of entry to and use of space are reduced. In all orbital regimes, especially low Earth orbit (LEO), preparation to respond quickly when the next breakup occurs is critical. This research utilizes high-performance parallel computation along with python-driven Systems Tool Kit (STK) to model a large-scale on-orbit breakup in LEO, with the goal of returning data in less than 90 minutes. The breakup is characterized by the National Aeronautics and Space Administration (NASA) EVOLVE 4.0 breakup model and is both dialable and scalable.

The debris field is analyzed over the course of one week using Gabbard plots. The risk posed by the breakup is determined using STK's Advanced Close Approach Tool (ACAT) to report minimum range, minimum separation, and likelihood of collision between the debris and catalog. The field is screened for close approaches each day of the week and the probability of collision is computed using multiple conjunction models (Alfano, Patera, Chan, Alfano Max) to observe how different models predict the likelihood of collision. The goal is to take steps towards preparing to respond to breakup events in the future.

Over the course of the analysis week, there were over 700,000 close approaches reported within three kilometers. ~11% of these approaches were reported within one kilometer. The average likelihood of at least one of the reported collisions happening daily was found to be 4.1% for the first three models and 22.3% for the maximum likelihood model.

Acknowledgments

To my amazing wife, I love you more than words can say and there is no way that I am here without you. I would contend that my greatest achievement at AFIT was adding a new member to our family.

To my daughter, this thesis may be a great accomplishment, but it pales in comparison to raising a child. My hope is that this endeavor has gifted you a bit more knowledge of astrodynamics than the average toddler.

To Colonel Fuller, I want to express my sincere gratitude for your guidance and mentorship throughout the course of this thesis work. You helped me truly enjoy my time at AFIT.

To the members of my committee, thank you for providing clarity and direction when I needed it most.

To my office mates, you guys rock and I can't have imagined a better group to banter with on a weekly basis.

To the colony, thank you for letting me vent and ruin your whiteboards when I ran into issues.

To the DSRC, thank you for your computer science expertise and enabling my parallel scripting capability.

Finally, to Analytical Graphics Incorporated, thank you for trusting me with the keys to your software. STK is the cornerstone of this work and I appreciate the opportunity to give it a workout.

David J. Buehler, 2nd Lieutenant & STK Grand Master

Table of Contents

Page

Abstract iv
Table of Contents vi
List of Figures viii
List of Tables x
I. Introduction 1
1.1 Background 1
1.2 Problem Statement & Hypothesis 5
1.3 Research Objectives 7
1.4 Research Questions 8
1.5 Assumptions, Scope, and Limitations 8
1.6 Methodology 10
II. Literature Review 12
2.1 Chapter Overview 12
2.2 Space Debris 12
2.3 Debris Field Characteristics 20
2.5 Space Object Position Uncertainty 24
2.6 Collision Probability Models 25
2.7 Summary 36
III. Methodology 38
3.1 Chapter Overview 38
3.2 General Methodology 39
3.3 Code Breakdown 46

3.4 Data Analysis Techniques 49

IV. Analysis and Results 52

4.1 Chapter Overview 52

4.2 Debris Field Characterization 52

4.3 Debris Features 60

4.4 Close Approach Tool Results 62

4.5 Summary 71

V. Conclusion and Recommendations 72

5.1 Chapter Overview 72

5.2 Review of Research Objectives 72

5.3 Research Question Answers 74

5.4 Recommendations 77

5.5 Conclusion and Future Work 77

Appendix A: Supplemental Charts 80

Appendix B: SGI ICE X (Thunder) System Specifications 81

Appendix C: Creating Custom Report Styles in STK 82

Bibliography 85

SF-298 88

List of Figures

Page

Figure 1. Depiction of all on-orbit cataloged objects 1

Figure 2. Object density inclination plot..... 6

Figure 3. Spatial density altitude plot for the LEO regime..... 6

Figure 4. 40-centimeter diameter damage to solar panel caused by millimeter-sized debris 14

Figure 5. Satellite catalog as of 29 December 2017 19

Figure 6. Estimated rate of decay of the FY-1C antisatellite test debris field..... 20

Figure 7. Debris belt formed after a breakup with annotated pinch point 21

Figure 8. Debris propagation of the FY-1C antisatellite test..... 22

Figure 9. An illustration of a close approach assuming linear relative motion 26

Figure 10. The conjunction simplified into a two-dimensional encounter 27

Figure 11. Modified encounter plane..... 31

Figure 12. An example close approach where the linear relative motion assumption does not apply..... 36

Figure 13. Job submission for supercomputer. number of nodes requested is 1, 36 is the number of CPUs per node, and 4 is the number of processes per node. 44

Figure 14. Running job on the supercomputer..... 45

Figure 15. Activity diagram for breakup simulation 46

Figure 16. 250-piece breakup scenario visualization..... 47

Figure 17. UML class diagram of research methodology..... 48

Figure 18. Gabbard plot for DMSP 5D-2/F13 50

Figure 19. Gabbard plot for Day 1 data 53
Figure 20. Gabbard plot for Day 7 data 54
Figure 21. Gabbard plot of debris pieces within LEO period. 56
Figure 22. Gabbard plot of FY-1C ASAT test 57
Figure 23. Modified Gabbard plot Day 7 data 58
Figure 24. Modified Gabbard plot constrained to 4,000-kilometer ceiling 59
Figure 25. FY-1C debris field spread over two years 62
Figure 26. Top-level distribution of minimum range zones for analysis week 64
Figure 27. Histogram of minimum range encounters for analysis week 65
Figure 28. Top-level distribution of minimum separation zones for analysis week 66
Figure 29. Histogram of minimum separation encounters for analysis week 68
Figure 30. Day 1 constrained modified Gabbard plot 80
Figure 31. Locating the report and graph manager 82
Figure 32. Locating the create new report style icon 83

List of Tables

Page

Table 1. Different sizes, quantities, and impact of space debris 13

Table 2. Representation of the different types of space debris 15

Table 3. Top ten breakups as of May 2010 15

Table 4. Maximum percent error for approximations 35

Table 5. Debris piece characteristic statistics 60

Table 6. Nodal precession statistics over time 62

Table 7. Top-level statistics for the different likelihood models 69

Table 8. Thunder Specification Charts 81

UTILIZING SUPERCOMPUTING TO ANALYZE RISKS OF AN EMERGENT LARGE-SCALE DEBRIS FIELD IN LOW EARTH ORBIT

I. Introduction

1.1 Background

It is currently estimated that there are several million pieces of debris in space. This debris ranges in size from as small as one millimeter flecks of paint to as large as a dead satellite body weighing nearly 18,000 pounds [1], [2]. Since 1961, there have been over 290 estimated on-orbit fragmentation events [3]. For reference, Figure 1 below is a depiction of all current cataloged objects [4].

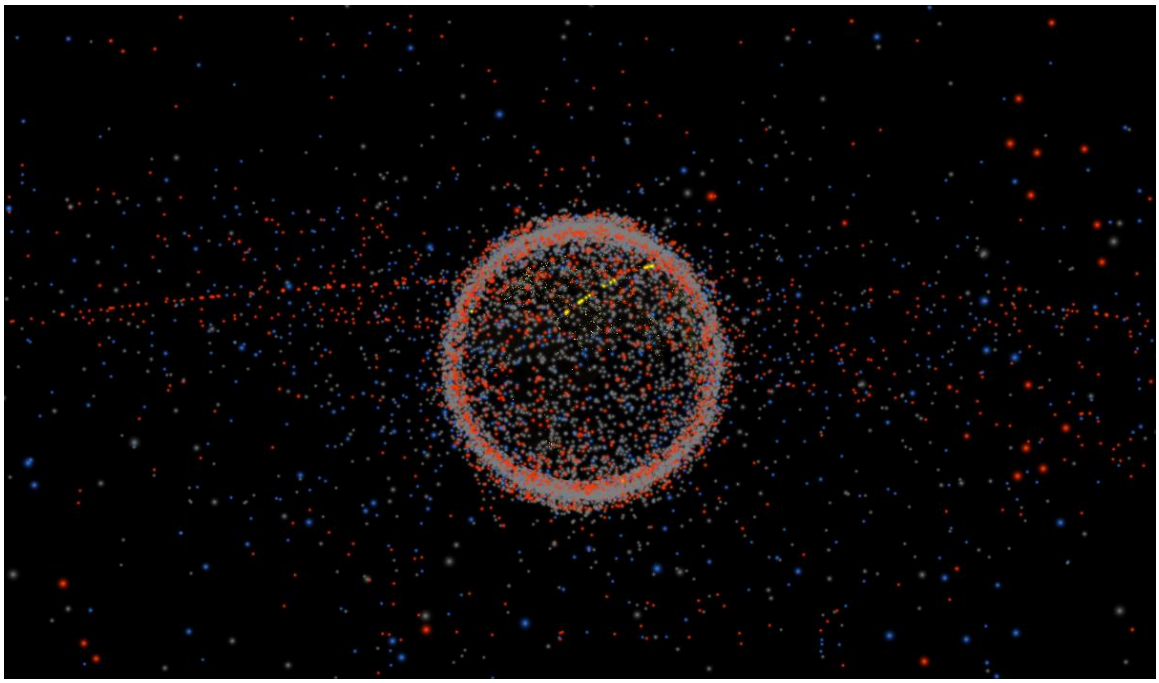

Figure 1. Depiction of all on-orbit cataloged objects

This debris poses a serious and persistent threat to United States (US) and civilian space assets. Arguably, the most dangerous pieces of debris are the pieces that have not yet materialized. That is, debris as the result of a sudden unexpected collision or explosion in space. It will likely take months to track down and catalog all the pieces of debris from a sudden breakup, and that still only accounts for the pieces that are large enough to track. In LEO, the time to respond to such breakup events is on the order of minutes. With such a short reactionary period, it is imperative to understand the threat ahead of time to be able to make an informed decision that could have substantial implications on the life and mission of a space asset.

Space debris falls under the broad umbrella of space situational awareness (SSA), which has been defined as, "Cognizance of the requisite current and predictive knowledge of the space environment and the operational environment upon which space operations depend [5]." Traditional SSA involves keeping track of known objects to understand their purpose and identify threats. With a sudden breakup however, the threat develops rapidly, fitting into the predictive aspect of SSA. Cognizance is important, but preparation to respond to such events is of equal importance. By taking steps towards understanding what the enemy could look like, we are better equipped to protect assets and not fall victim to the emergent threat.

Additionally, with the advent of cubesats and reusable rocket stages, the barrier to entry for space continues to be driven lower. This means more players and more chances for failure. Some suggest that this barrier is dropping so rapidly that the space industry will be worth over three trillion dollars within three decades [6]. While other research is

being conducted to study protective measures such as spacecraft hardening, the focus of this research is on studying the risks of an emergent debris field on current spacecraft.

Debris Field Characteristics

While each breakup will be different in terms of magnitude and cause, steps have been taken to begin characterizing the way debris fields behave. The initial expansion of a debris field looks much like a conventional explosion in that it expands in spherical fashion from the point of breakup. This point is known as the pinch point, and every debris piece generated will share this point in their new orbits. The way this expansion behaves is dependent on the cause of the breakup, whether it be from a sudden internal explosion, collision, or even antisatellite weapon. Regardless of the initial expansion, the debris field will begin to stretch to form a dense belt over the next month, impacting multiple altitudes. As months pass, the oblateness of the Earth will cause the node of the pieces to precess, further impacting a larger number of orbit planes. This causes an interesting paradox in that the odds are lower for any one piece of debris being involved in a collision (due to the spread of the field), however the overall odds of collision in general have been raised due to the overall increase in background spatial density [7]. By the time all the debris has been cataloged, it may have already caused other breakups [8]. Based on all the information above, it can be reasonably stated that the critical time to react to a breakup in LEO is within the first week, as this is when the debris field is most densely concentrated.

Cascading debris fields have become a topic of concern as the satellite catalog continues to balloon. More commonly known as Kessler Syndrome [9], the concept is

that one collision would produce debris that would cause another collision shortly after. This would ultimately turn LEO into a densely-packed debris graveyard. This topic will be further discussed in Chapter 2. There are no winners when debris begins to cascade and it is everyone's responsibility to protect the space environment which affords many things we consider necessities (GPS, global communication, weather forecasts, etc.). Regardless of the next source of debris, it is critical to have a plan to avoid being the next domino in the cascade.

Close Approach Analysis

When objects in space are predicted to pass each other within a defined miss distance, a close approach analysis is launched. This can be accomplished using several methods that are described in detail in Chapter 2. This analysis results in a likelihood of collision that is reported to satellite operators. The Joint Space Operations Center (JSpOC) at Vandenberg AFB provides satellite operators with collision warnings for near miss distances less than one kilometer in LEO and less than five kilometers in geosynchronous orbit (GEO). These warnings come at an average of thirty per day and the day-to-day statistical chance of collision is around $1e^{-6}$. This information is passed to operators within 72 hours prior to the expected event occurrence and it is the operator's decision whether or not to perform a collision avoidance (COLA) maneuver [10]. For many satellites, maneuvering may not even be an option for a number of reasons (short mission life, not enough payload space for a propellant system, etc.). Aside from JSpOC, who issues warnings free of cost, there are additional commercial options which provide the customer with the "premium" version of the JSpOC warning system.

1.2 Problem Statement & Hypothesis

As space continues to grow more congested and contested [5], it is critical to be prepared for the next inevitable collision or explosion. As stated in section 1.1, every debris field will be different in terms of scope, cause, and location. Rather than model a large number of fields, this research focusses on one particular initial state (850 km altitude | 83° inclination). This altitude and inclination was chosen for study as it is one of the densest regions in the catalog. This is validated below by Figure 3 from an early 2017 presentation by NASA to the Committee on the Peaceful Uses of Outer Space and by Figure 2 from *Orbital Debris A Technical Assessment* [11], [12]. In Figure 3, the impact from the two largest breakup events on the density is clear. One of the biggest issues with modeling a high-fidelity debris scenario is the sheer computational power needed. To take a computationally-heavy number of objects, propagate the orbits for any length of time, and run a close approach analysis is a tall order for almost all conventional computers.

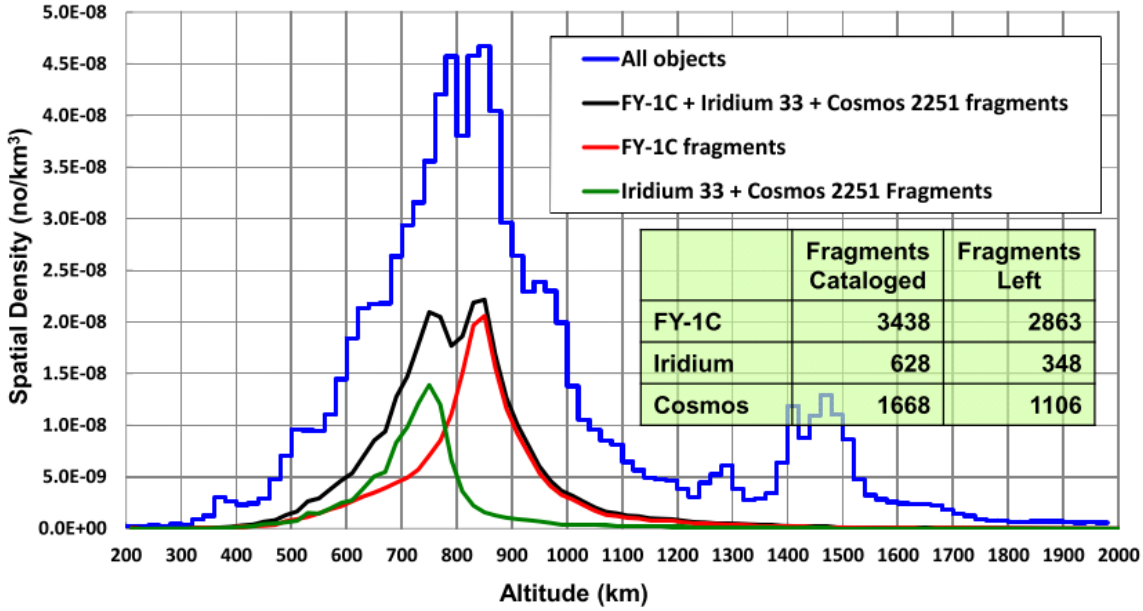

	Fragments Cataloged	Fragments Left
FY-1C	3438	2863
Iridium	628	348
Cosmos	1668	1106

Figure 3. Spatial density altitude plot for the LEO regime

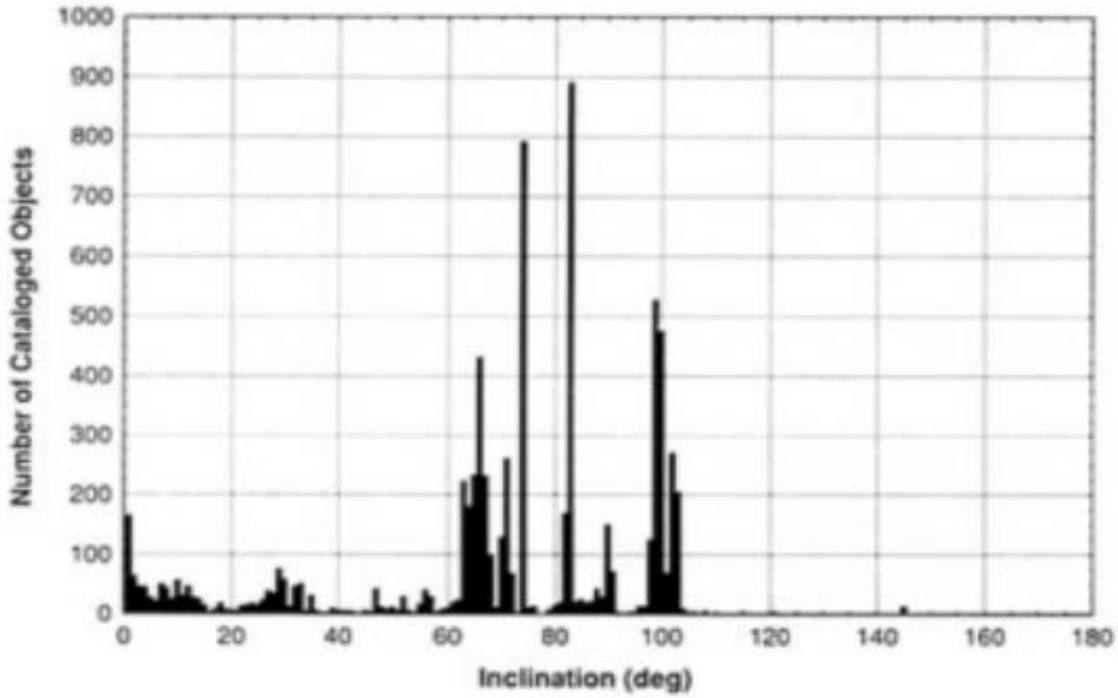

Figure 2. Object density inclination plot

The combination of these issues leads to the problem statement for this research:

- **Problem Statement:** Modeling large-scale breakup events with any sort of fidelity requires a substantial amount of computational power. It is possible to analyze small scale debris events with conventional computation, but it remains to be seen if parallel-computation can be utilized to model and analyze large-scale breakup scenarios on an operational timeline.

This problem statement then drives the hypothesis:

- **Hypothesis:** A supercomputer can be utilized to simulate and analyze a large-scale on-orbit breakup scenario on an operational timeline.

The term "operational timeline" is used to describe the time from beginning the scenario to receiving the data. The goal for this research is to simulate, analyze, and report results within an average LEO period (90 minutes).

1.3 Research Objectives

As stated previously, the first week of a breakup is high risk and full of unknowns. The object(s) involved, cause of breakup, and scope are still being determined. Over the course of one week, an average LEO satellite (period ~90 mins) will make approximately 112 orbits, each with a chance to cross paths with a newly-formed piece of debris. The unknowns in the time following a breakup have led to the following research objectives:

- **Research Objective #1:** Model a large-scale (100,000 pieces) debris field, propagated for one week, utilizing parallel computing on the supercomputer.

- **Research Objective #2:** Perform a close-approach analysis using the ACAT to report the number of close approaches, minimum range and separation, and likelihood of collision of the generated debris with the current catalog of on-orbit objects over the course of one week.
- **Research Objective #3:** Perform all the above and provide results within 90 minutes.

1.4 Research Questions

Over the course of this research, the goal is to ultimately provide an answer to the following questions:

- **Research Question #1:** How can massively-parallel computation on the supercomputer be used to model large-scale debris events in STK?
- **Research Question #2:** How can the risk involved with the aforementioned debris event be quantified using STK's ACAT?
- **Research Question #3:** How can the computation time be reduced to meet an operational timeline?

These questions will be reassessed in the conclusion of this thesis.

1.5 Assumptions, Scope, and Limitations

As stated previously, this research examines a breakup event at an altitude of 850 km and an inclination of 83°. Additionally, this altitude and inclination were chosen as this is where the greatest spatial density of objects is. The full initial state of the parent orbit is defined below:

- Circular orbit (eccentricity = 0)
- Altitude = 850 km
- Inclination = 83°
- Right Ascension of Ascending Node = 0°
- Argument of Periapsis = 0°
- Mean Anomaly = 0°

The scope of the event has been limited to 100,000 pieces and can be scaled to account for any size field. The debris pieces are assumed to be spherical aluminum pieces, with the minimum diameter incorporated being set at three millimeters and the maximum diameter set at one meter. The minimum and maximum diameter are scalable. The coefficients of drag, solar radiation pressure (spherical), and radiation pressure (albedo/thermal) are set at the STK standard of 2.2, 1, and 1 respectively. It is assumed the cause of the breakup is an undefined internal failure (electrical, propulsion, etc.). The pieces are propagated for one week or until the altitude drops to 120 kilometers, at which point the debris is assumed to have reentered and is removed from the scenario. The propagator being used is STK's internal High-Precision Orbit Propagator (HPOP) v10. This propagator's characteristics are listed below:

- Gravitational force from central body
- Drag with Jacchia-Roberts atmospheric density model
- Spherical Solar Radiation Pressure (SRP)
- Sun and Moon third-body forces

- Runge-Kutta-Fehlberg integration method of 7^{th} and 8^{th} order error control for integration step size

The ACAT close approach threat sphere for each debris piece is set at one kilometer in the x, y, and z direction centered on the debris piece and can be changed as desired. This was chosen as it is the current warning threshold for JSpOC. A close approach warning is triggered when the threat sphere of any object passes within one kilometer of the threat sphere of a debris piece.

This research is limited to a LEO breakup and the characteristics of the resulting debris field are limited by the assumptions within the NASA EVOLVE 4.0 breakup model, which is discussed in detail in Chapter 3. The scenario is limited to one week, but could be expanded as long as desired with increasing computational burden to account for the additional propagation time.

1.6 Methodology

This research seeks to take first steps towards defining an operations plan for responding to on-orbit breakups. The first step in this definition process is to accurately model an on-orbit breakup. Once the model has been defined, a close approach analysis will be run to evaluate the relative risk posed by the breakup on the rest of the catalog. The final step of such a plan would be to define a prescribed course of action to the breakup. This would require an analysis and optimization of possible maneuvers to reduce the risk of collision to a desired probability. This research will explore the first half of this plan, defining the debris field and performing the close approach analysis.

Python coding and space modeling skills learned at the Air Force Institute of Technology are utilized to simulate an on-orbit breakup and study it over the course of one week. Additionally, this research utilizes STK in conjunction with one of the Defense Supercomputing Resource Center's supercomputers at Wright Patterson Air Force Base to drastically reduce the computational time from many hours to operational levels. Finally, the simulated debris field is analyzed for close approaches with the catalog of on-orbit objects. The debris field is characterized with Gabbard plots and classical orbit element reports. The number of close approaches and probabilities of collision will be presented per day for the analysis week. The following chapter will discuss in detail the literature that relates to each aspect of this research.

II. Literature Review

2.1 Chapter Overview

The purpose of this chapter is to provide a detailed background on the topics that relate to and support this research. Section 2.2 gives a historical account of space debris. In this section, major debris events, dangers to spacecraft, and the current state of debris mitigation strategy will be discussed. Following the debris background, a more technical discussion of space debris generation is presented in section 2.3. This section will revolve around the traits of a debris field with a discussion on how the debris is formed, settles into its new orbit, and expands over time. Section 2.4 provides a brief discussion on spacecraft maneuverability. Section 2.5 will discuss location uncertainty of spacecraft. This chapter concludes with section 2.6 with a presentation of the different collision likelihood models.

2.2 Space Debris

This section serves as an overview of space debris. It covers the background of space debris, a brief history of debris mitigation and policy, and concludes with a discussion on the current state of space debris and the future debris environment.

Space Debris Background

Space debris has been defined by the United Nations Office for Outer Space Affairs as any manmade object in earth orbit or reentering the atmosphere, that is nonfunctional [13]. As of February 2018, there were 18,950 objects in the on-orbit space catalog, of which 75% are debris and rocket bodies [14]. In January 2007, the worst breakup to date occurred as a result of the Fengyun-1C (FY-1C) antisatellite test. The

explosion, which occurred at 865 kilometers, instantly added more than 3,400 trackable (>10cm) objects to the catalog. In February 2009, just two years after the FY-1C incident, Iridium 33 and Cosmos 2251 collided at an altitude of just under 800 kilometers generating more than 2,200 trackable pieces of debris. These two debris events alone increased the catalog size by 65% [7].

Arguably more dangerous are the estimated hundreds of thousands of currently untrackable (<10 cm) objects. Untrackable may be a bit of a misnomer, as it is possible to track objects down to 1 cm. Mostly however, these objects are rarely tracked and only with a limited specialized set of sensors. Additionally, objects around this size will more than likely not cause fragmentation or be massive enough to propagate Kessler syndrome. Objects this small currently go mostly undetected and can act as bullets flying at speeds of well over 15,000 mph in LEO. These objects, while unlikely to cause catastrophic breakups, can still wreak havoc on mission-critical subsystems. Table 1 below is a table describing the different sizes, estimated quantities, and impact of debris pieces.

Table 1. Different sizes, quantities, and impact of space

Debris size	Quantity	Impact
1 mm to 3 mm	Millions	• Cannot be tracked • Localized damage
3 mm to 1 cm	Millions	• Cannot be tracked • Localized damage • Upper limit of shielding
1 cm to 5 cm	500,000 (estimated)	• Most cannot be tracked • Major damage
5 cm to 10 cm	Thousands	• Lower limit of tracking • Catastrophic damage
10 cm or larger	Hundreds to low thousands	• Tracked and cataloged by space surveillance network • Catastrophic damage

To put a picture to the words above, the 40-centimeter diameter damage to the solar panels shown in Figure 4 below occurred on 31 August 2016 when the Copernicus Sentinel A-1 satellite was struck by a millimeter-sized piece of debris [15].

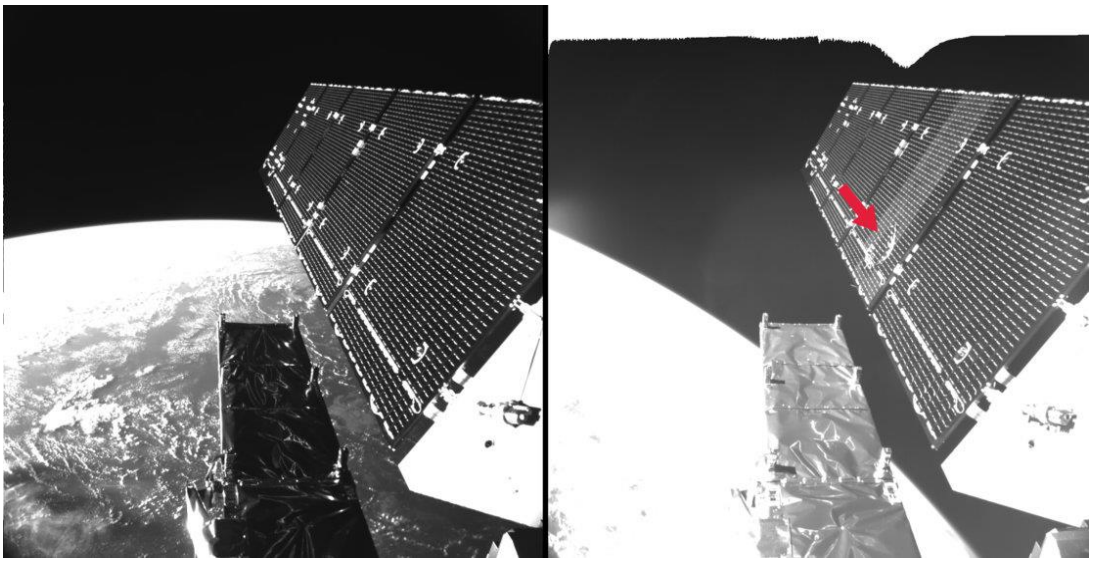

Figure 4. 40-centimeter diameter damage to solar panel caused by millimeter-sized debris

With the Air Force Space Fence on Kwajalein expected to come online in 2019, some of the untrackable debris objects will be revealed. With the improved capabilities, it is anticipated that the catalog will balloon to at least 200,000 objects [16]. Space debris comes in many shapes and sizes, from large derelict satellites [1] and rocket bodies to centimeter-sized drops of liquid metal [17] and millimeter-sized flecks of paint [18]. Table 2 on the following page gives an excellent summary of the various forms that debris presents itself in [7].

Table 2. Representation of the different types of space debris

Debris size	Mass (g) aluminum sphere	Kinetic Energy (J)	Equivalent TNT (kg)	Energy similar to
1 mm	0.0014	71	0.0003	Baseball
3 mm	0.038	1910	0.008	Bullets
1 cm	1.41	70,700	0.3	Falling anvil
5 cm	176.7	8,840,000	37	Hit by bus
10 cm	1413.7	70,700,000	300	Large bomb

Debris can be generated by collisions like Iridium/Cosmos, antisatellite weapons like FY-1C, scientific experiments like the West Ford needles experiment [19], or simply by a non-responsive satellite. Historically however, it comes from exploding defunct rocket bodies. There are a number of causes for the eventual explosion of these rocket bodies, but the primary cause is remnant fuel. Table 3 below was compiled by NASA and shows the top ten breakups as of May 2010, where it is clear that more than half were caused by rocket body explosions [20].

Table 3. Top ten breakups as of May 2010

Common Name	Year of Breakup	Altitude of Breakup	Cataloged Debris*	Debris in Orbit*	Cause of Breakup
Fengyun-1C	2007	850 km	2841	2756	Intentional Collision
Cosmos 2251	2009	790 km	1267	1215	Accidental Collision
STEP 2 Rocket Body	1996	625 km	713	63	Accidental Explosion
Iridium 33	2009	790 km	521	498	Accidental Collision
Cosmos 2421	2008	410 km	509	18	Unknown
SPOT 1 Rocket Body	1986	805 km	492	33	Accidental Explosion
OV 2-1 / LCS 2 Rocket Body	1965	740 km	473	36	Accidental Explosion
Nimbus 4 Rocket Body	1970	1075 km	374	248	Accidental Explosion
TES Rocket Body	2001	670 km	370	116	Accidental Explosion
CBERS 1 Rocket Body	2000	740 km	343	189	Accidental Explosion
			Total: 7903	Total: 5172	

* As of May 2010

Debris Mitigation Strategies and Policy

Space debris received its first official study in 1988 by the United Nations Committee on Space Research [21]. Following this research, mitigation strategies were proposed by NASA in 1995 with the publishing of NASA Safety Standard 1740.14 *Guidelines and Assessment Procedures for Limiting Orbital Debris.* In this standard, NASA addressed five main issues:

- Debris released during normal operations
- Debris generated by explosions and intentional breakups
- Debris generated by on-orbit collisions during mission operations
- Safe disposal of space systems after mission completion
- Structural components impacting the Earth following postmission disposal by atmospheric reentry [22]

Many mitigation statements and strategies have since been drafted and refined, with the most current U.S. space policy stating, "Preserve the Space Environment. For the purposes of minimizing debris and preserving the space environment for the responsible, peaceful, and safe use of all users, the United States shall:

- Lead the continued development and adoption of international and industry standards and policies to minimize debris, such as the United Nations Space Debris Mitigation Guidelines;
- Develop, maintain, and use space situational awareness (SSA) information from commercial, civil, and national security sources to detect, identify, and attribute

actions in space that are contrary to responsible use and the long-term sustainability of the space environment;

- Continue to follow the United States Government Orbital Debris Mitigation Standard Practices, consistent with mission requirements and cost effectiveness, in the procurement and operation of spacecraft, launch services, and the conduct of tests and experiments in space;
- Pursue research and development of technologies and techniques, through the Administrator of the National Aeronautics and Space Administration (NASA) and the Secretary of Defense, to mitigate and remove on-orbit debris, reduce hazards, and increase understanding of the current and future debris environment; and
- Require the head of the sponsoring department or agency to approve exceptions to the United States Government Orbital Debris Mitigation Standard Practices and notify the Secretary of State [23]."

The same year this space policy was released, the United Nations released a set of guidelines for debris mitigation based on the findings of the Office of Outer Space Affairs. In the document, the UN highlights seven guidelines for mitigation. They are as follows:

- Limit debris released during normal operations
- Minimize the potential for break-ups during operational phases
- Limit the probability of accidental collision in orbit
- Avoid intentional destruction and other harmful activities
- Minimize potential for post-mission break-ups resulting from stored energy

- Limit the long-term presence of spacecraft and launch vehicle orbital stages in the low-Earth
- Limit the long-term interference of spacecraft and launch vehicle orbital stages with the GEO region after the end of their mission [13]

The language in the guidelines is telling. Of particular interest is the choice of words that begin each guideline (limit, minimize, and avoid), which indicate that the problem cannot be eliminated altogether, but instead space-faring entities must "do their best" to adhere. Additionally, comparing these guidelines to the NASA guidelines of 1995 shows that the core of mitigation strategy has not changed in over a decade and breakups are still occurring at a rate of about four per year as of 2015 [2]. Debris-mitigation strategy will continue to improve as time goes on and there may even be ways to decontaminate space in the future [24]. However, for the time being, it is imperative to be a defensive driver in space and always be prepared for the unexpected.

Debris Cascades and the Future of Debris

As stated previously, the recent advent of reusable rocket stages has driven the barrier to entry for space lower. As the number of space-faring nations and companies grows, the days of big space/small satellite being a collision-avoidance strategy are no longer. It was first theorized by Donald Kessler and Burton Cour-Palais in their 1978 paper, *Collision Frequency of Artificial Satellites: The Creation of a Debris Belt*, that future collisions could generate enough debris to cause an exponential increase in debris flux. Eventually, this flux will become so great that it will continue to grow unchecked.

This will ultimately form a shell of debris around the earth, rendering LEO a graveyard, useless for satellite operations and preventing launches to MEO and beyond [25].

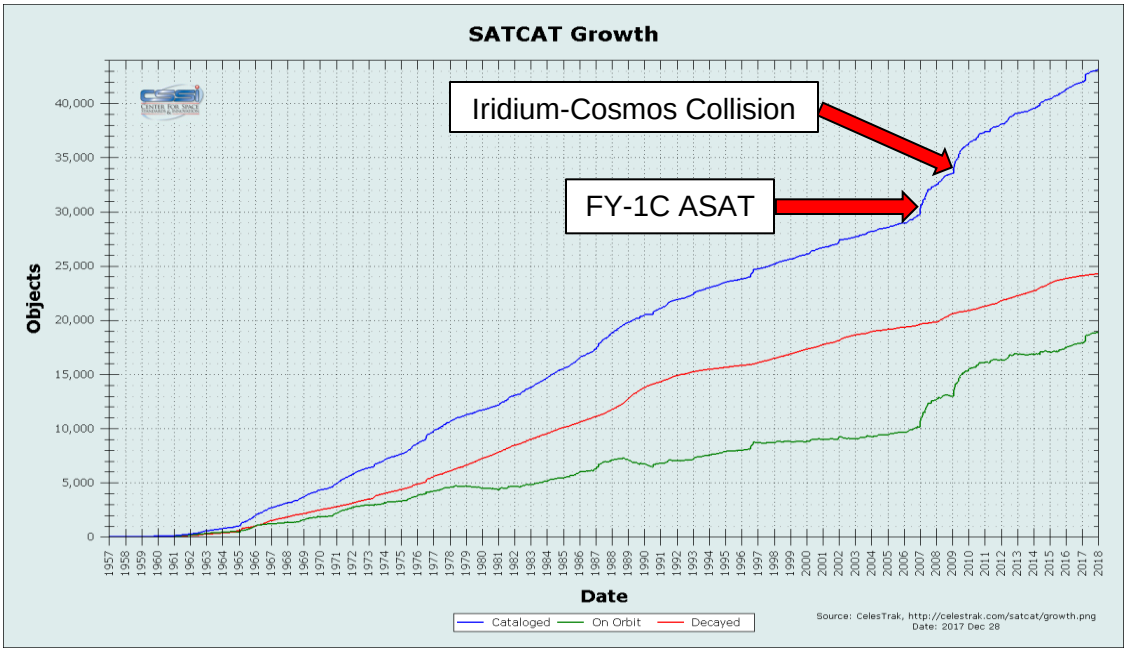

Figure 5. Satellite catalog as of 29 December 2017

Figure 5 above depicts the growth of the satellite catalog as of December 2017 [26]. It is clear from this graph that the number of objects, both debris and active satellites, is continuing to grow at a substantial rate. Counter to the substantial rate of growth is the slow rate of decay. Figure 6 on the following page shows the estimated rate of decay of the debris from the FY-1C antisatellite test. It can be seen that only one fifth of the debris is expected to decay within 90 years of the breakup [27]. With the rate of growth of the catalog, coupled with the amount of uncontrollable debris and slow decay rates, the question is not if another breakup will happen, but when.

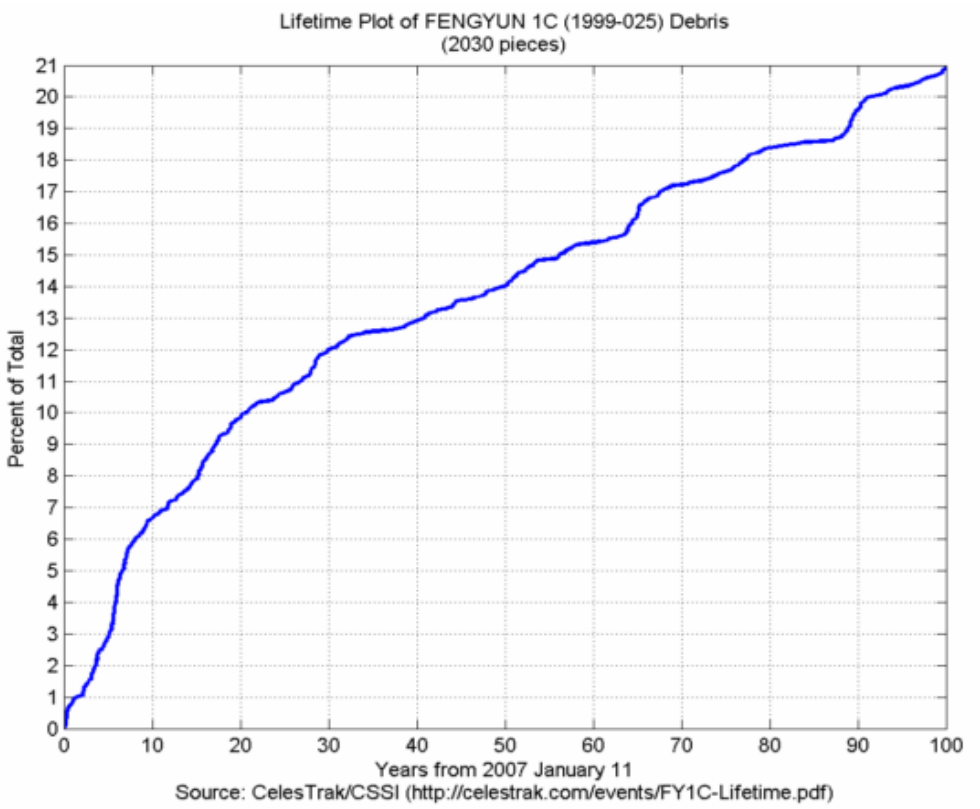

Figure 6. Estimated rate of decay of the FY-1C antisatellite test debris

2.3 Debris Field Characteristics

This section describes the characteristics of a debris field. It begins with a discussion of the initial characteristics of a debris field and continues with a discussion on the evolution of this debris field over time.

Initial Breakup

When a breakup occurs, the debris will initially expand into a spherical cloud. Each piece of debris enters a new orbit determined by a number of elements including initial velocity of the parent, spreading velocity magnitude and direction imparted by the breakup, etc. Depending on the altitude, many pieces may reenter Earth's atmosphere almost instantaneously due to their relative velocity being in the direction of the Earth.

As the pieces continue into their new orbital trajectory, they begin to fan out creating what appears to be a belt of debris. The most dangerous part of this belt is at the pinch point, the point of initial breakup. The pinch point in the orbit is shared by all pieces of debris, making it the most likely place to intersect. The initial debris belt with the pinch point highlighted is shown below in Figure 7.

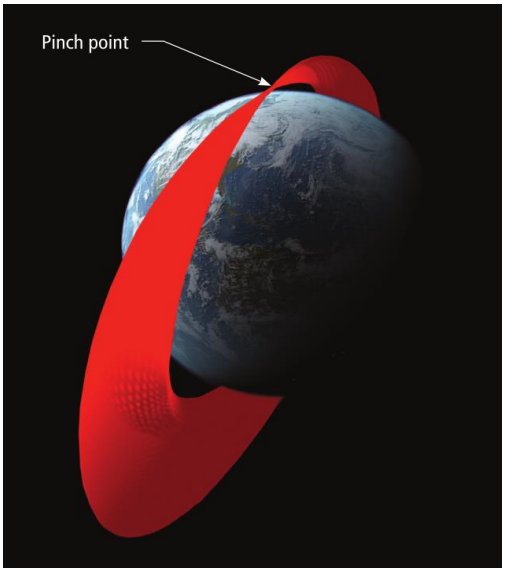

Figure 7. Debris belt formed after a breakup with annotated pinch point

Breakup Expansion

Analysis of previous breakups reveals that as time goes and the debris experiences the nodal precession effects of the oblateness of Earth, the pieces will spread and affect other orbit regimes [28]. This will create a shell of debris that, while less concentrated, increases the overall background spatial density [7]. A visualization of this propagation for the FY-1C antisatellite test, including the long-term debris shell, is shown in Figure 8 on the following page [29]–[32]. This expansion also begins to infringe on launch windows, cutting precious minutes out when the risk is deemed too severe.

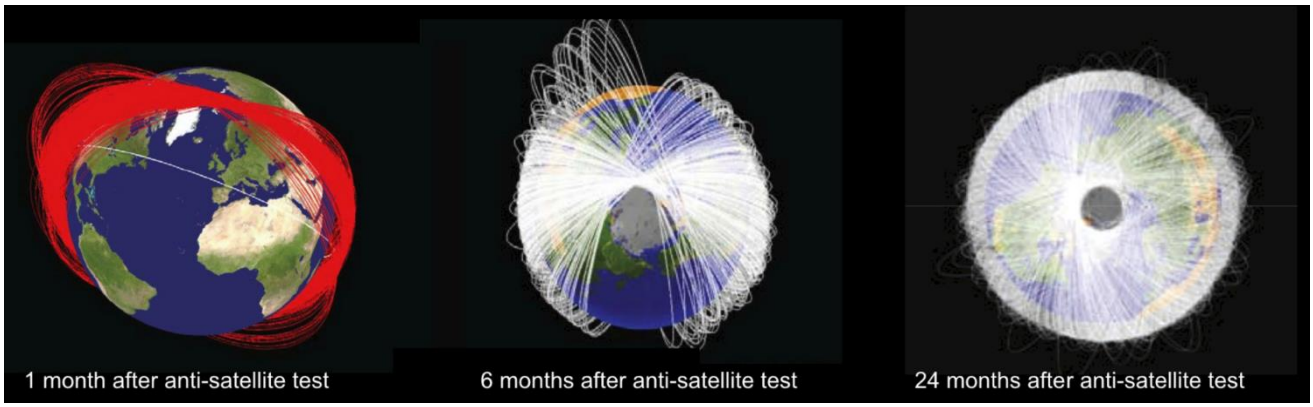

Figure 8. Debris propagation of the FY-1C antisatellite test

2.4 Spacecraft Maneuvering

Deciding whether to maneuver a satellite can be a difficult decision to make, as fuel determines a satellite's mission life. This is especially true in LEO, where Earth's effects induce large perturbations in orbits that require station-keeping to keep the satellite in the desired orbit. Maneuvering a satellite can also have massive implications on mission effectiveness. For example, a change in orbit altitude or inclination may have noticeable consequences in missions with precise equipment like remote sensing. In addition to maneuvering, per US Government Orbital Debris Mitigation Standard Practices, a satellite must be deorbited within 25 years of mission completion. This can be accomplished through a controlled reentry burn or the use of a drag enhancement device [33].

A particular case in which a satellite may be maneuvered is to avoid a close approach. Each satellite is different in terms of acceptable probabilities of conjunction. The International Space Station (ISS), being a manned spacecraft, has a much different

threshold than unmanned spacecraft. Specifically, there is a “pizza box” defined around the ISS that extends 2 kilometers above and below as well as 25 kilometers in-track and 25 kilometers cross-track. If anything is expected to enter the box, flight controllers are alerted and begin assessing probabilities of collision. If the probability of collision is between 1 and $1e^{-4}$, the threshold is called red. In red, the station will always be maneuvered unless maneuvering places the crew at additional risk. Probabilities between $1e^{-4}$ and $1e^{-5}$ are deemed yellow. In yellow cases, the station is maneuvered unless a maneuver impacts the mission negatively [34].

For unmanned spacecraft, the decision to maneuver will be made on a case-by-case basis. For most spacecraft, the decision is a simple one as there is no onboard thruster system. Additionally, as previously stated, requirements dictate that a portion of onboard fuel be reserved for deorbit burns, meaning unplanned burns must be well thought out. An extreme case is exemplified by NASA’s Fermi Gamma-ray telescope. On 29 March 2012, the Fermi team was notified of a likely 700-foot close approach with Cosmos 1805, a dead Soviet-era spy satellite. A maneuver was clearly necessary, but the issue was that Fermi was never intended to maneuver during the mission life at all. All fuel onboard was in place for the sole purpose of reentry burning. With the high relative speed of Cosmos 1805, the magnitude of the collision would have created hundreds of thousands of pieces of debris. Based on the collision analysis, the risk of a slightly longer decay period was the lesser of the two evils. The Fermi team would opt to perform a one second impulsive burn five days later, resulting in a miss distance of about ten kilometers [35].

2.5 Space Object Position Uncertainty

Locating and tracking space objects presents unique challenges. While this research is not a study in positional covariance, it should still be discussed as it is an important part of close approach analysis. Specifying the nitial location of a known object may not be difficult, but this task becomes exponentially harder when presented with a breakup. Locating objects in this case is a race to provide operators with time-sensitive close approach data to help with informed decision-making regarding maneuvering. To give some historical context, it took roughly two weeks for less than 25% of the FY-1C debris to be tracked down and catalogued [27]. Some quick math reveals that a typical LEO satellite would have completed over 200 orbits in the time it took to track down this fraction of the debris.

Besides locating an object in space, a more difficult task is then predicting where that object will be in the future. At first glance, this does not appear too daunting a task, but in LEO the Earth's oblateness and topography can lead to large perturbations in orbit determination. When propagating orbits in LEO, uncertainty in air drag, force modeling, initial conditions, among other factors will greatly reduce the accuracy of orbit propagation within days in some cases. Because of this, two-line element (TLE) sets might be generated multiple times daily to ensure location accuracy. In GEO, outside of many of the Earth's effects, TLEs are more likely to be updated only as needed [36]. The most commonly used propagator is Simplified General Perturbations 4 (SGP4), which was created in 1970 by Ken Cranford and has since received several modifications to account for different circumstances [37]. The SGP4 propagator has been shown in at least

one study to give positional errors on the order of ten kilometers after just three days of propagation [38].

2.6 Collision Probability Models

In this section, the leading collision probability models will be discussed. The linear probability methods section below follows Salvatore Alfano's 2007 paper, *Review of Conjunction Probability Methods for Short-term Encounters* [39]. In this paper, Dr. Alfano presents a summary of the leading collision likelihood models. While not utilized in this research, non-linear collision probability models will be briefly discussed.

General Assumptions for Linear Probability Methods

Most collision analyses assume the spacecraft to be a sphere. When this assumption is made, there is no need to have information about the attitude of the spacecraft. Relative motion is generally considered to be linear in these analyses as well. Additionally, the relative velocity at the point of closest approach is assumed to be large enough to assume static covariance and a brief encounter. Positional error is assumed to be zero-mean, Gaussian, uncorrelated, and constant for the encounter. An encounter region is defined when one object is within n standard deviations of the combined covariance ellipsoid.

The uncorrelated covariance matrices can be summed to form one covariance ellipsoid centered on the primary object. The secondary object passes quickly through the ellipsoid in a tube-shaped path known as the "collision tube." An illustration of an encounter is shown below in Figure 9.

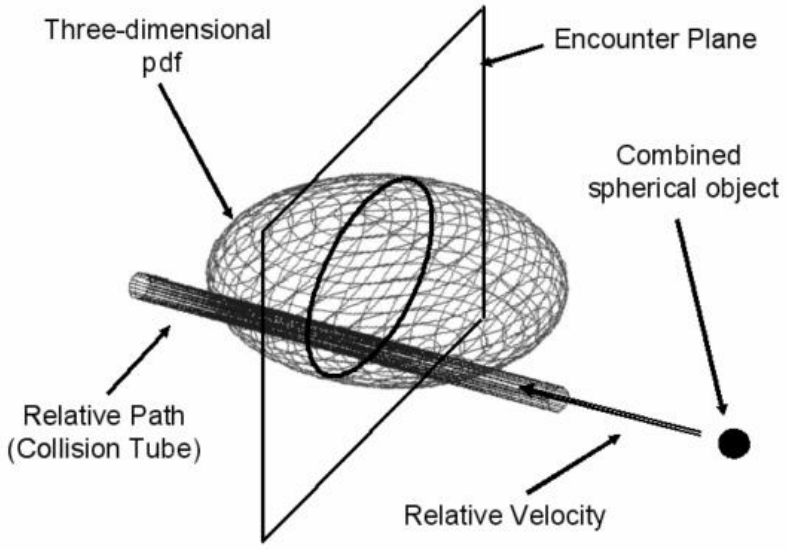

Figure 9. An illustration of a close approach assuming linear relative motion

For a short-term encounter, the tube can be assumed to be straight and is traversed quickly. Long-term encounters will typically only occur with GEO satellites in which close approaches can take a full day or longer to pass [40]. Due to the location of the breakup in this research being in LEO, only short-term encounters will be investigated. With this assumption, the encounter can be simplified to a two-dimensional plane visualized below in Figure 10.

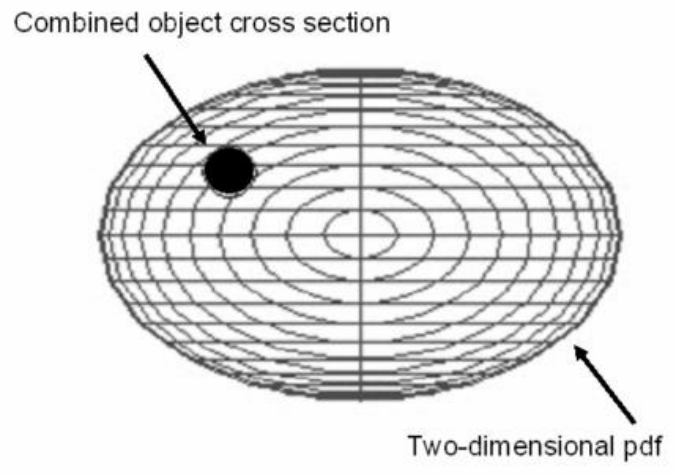

Figure 10. The conjunction simplified into a two-dimensional encounter

Physical overlap occurs if the secondary sphere comes within a distance equal to a sum of the two radii. The probability of collision is obtained by evaluating the integral of the three-dimensional probability density function (PDF) within a long circular cylinder. This is equivalent to evaluating the integral of the two-dimensional PDF within a circle on a plane perpendicular to the relative velocity at closest approach. The two-dimensional probability in Cartesian space is given below by Equation 1.

$$P = \frac{1}{2\pi\sigma_x\sigma_y}\int_{-OBJ}^{OBJ}\int_{-\sqrt{OBJ^2-x^2}}^{\sqrt{OBJ^2-x^2}} e^{-\frac{1}{2}\left[\left(\frac{x-x_m}{\sigma_x}\right)^2+\left(\frac{y-y_m}{\sigma_y}\right)^2\right]} dydx \qquad [1]$$

- OBJ = combined object radius
- x, y = minor and major axes respectively
- x_m, y_m = projected miss distance in the x and y direction respectively
- σ_x, σ_y = standard deviation in the x and y direction respectively

This equation is expressed via analytical approximation by Chan or numerically by Foster, Patera, and Alfano. These four methods will be detailed next.

Foster's Method

J. L. Foster's method uses polar coordinates in the encounter plane and is computed by the Equation 2 below.

$$P = \frac{1}{2\pi\sigma_u\sigma_w}\int_0^{OBJ}\left[\int_0^{2\pi} e^{\left[-\frac{1}{2}\left[\left(\frac{(R_0\sin(\phi)-r\sin(\theta)}{\sigma_u}\right)^2+\left(\frac{(R_0\cos(\phi)-r\cos(\theta)}{\sigma_w}\right)^2\right]\right]} r d\theta\right] dr \qquad [2]$$

- U, W = encounter plane principal axes
- σ_u, σ_w = standard deviation of the principal axes
- R = miss distance
- r = object radius
- θ = angle
- ϕ = miss distance relative to ellipse primary axis

Foster's method is used by NASA in determining on-orbit risk for the ISS and was also used for the Shuttle missions. It has also been used by Aerospace Corporation in their Collision Tool.

Patera's Method

Russell Patera's method takes Equation 1 and converts it to an equivalent one-dimensional line integral. Since the probability density is symmetrical, it enables the two-dimensional integral to be reduced to a one-dimensional path integral. This is expressed by Equation 3 below if the miss distance exceeds the combined object radius.

$$P = -\frac{1}{2\pi}\oint_{ellipse} e^{-\alpha r^2} d\theta \qquad [3]$$

If the combined object radius exceeds the miss distance, then it is expressed by Equation 4 below.

$$P = 1 - \frac{1}{2\pi}\oint_{ellipse} e^{-\alpha r^2} d\theta \quad [4]$$

Where:

- r = distance to the hardbody perimeter
- θ = covariance-centric angle position measured from the x-axis
- α = coefficient defining probability density (detailed computation of this term given in Patera's original paper [41])

This method is employed by several U.S. government organizations and civilian corporations.

Alfano's Method

Salvatore Alfano took Equation 1 and developed a series expression that is a combination of error functions and exponential terms. Within the encounter plane defined above, the combined object's center is located at x_m and y_m. This expression is shown below in equation 5.

$$P = \frac{2 \cdot OBJ}{\sqrt{8\pi}\sigma_x n}\sum_{i=0}^{n}\left[erf\left[\frac{\left[y_m + \frac{2 \cdot OBJ}{n}\sqrt{(n-i)\cdot i}\right]}{\sqrt{2}\sigma_y}\right] + erf\left[\frac{\left[-y_m + \frac{2 \cdot OBJ}{n}\sqrt{(n-i)\cdot i}\right]}{\sqrt{2}\sigma_y}\right]\right] \cdot e^{\left[-\frac{\left[\frac{OBJ(2i-n)}{n} + x_m\right]^2}{2\sigma_x^2}\right]} \quad [5]$$

- OBJ = combined object radius
- σ_x, σ_y = standard deviation in the x and y direction respectively

This method uses Simpson's one-third rule and breaks the series into m even and odd components. This m term is determined by Equation 6 below with a lower bound of 10 and an upper bound of 50.

$$m = int\left(\frac{5 \cdot OBJ}{\min\left(\sigma_x, \sigma_y, \sqrt{x_m^2 + y_m^2}\right)}\right) \quad [6]$$

Chan's Method

Ken Chan's Method uses a series expression as an analytical approximation to Equation 1. It uses the following representative present-day values.

- 1m ≤ OBJ ≤ 100m
- 10m ≤ miss distance ≤ 100km
- 1km ≤ σ ≤ 10 km

This method transforms the two-dimensional Gaussian PDF to a one-dimensional Rician PDF and uses equivalent areas. The probability is expressed by Equation 7 below centered at (x_m, y_m).

$$P = e^{-\frac{v}{2}} \sum_{m=0}^{\infty} \left[\frac{v^m}{2^m m!}\left(1 - e^{-\frac{u}{2}} \sum_{k=0}^{m} \frac{u^k}{2^k k!}\right)\right] \quad [7]$$

- OBJ = combined object radius
- σ_x, σ_y = standard deviation in the x and y direction respectively
- $u = \frac{OBJ^2}{\sigma_x \sigma_y}$
- $v = \frac{x_m^2}{\sigma_x^2} + \frac{x_m^2}{\sigma_y^2}$

Alfano's Maximum Probability Method

Salvatore Alfano created a method to solve for the absolute worst-case probability of collision for a particular event by finding the combined Gaussian probability density that maximizes the collision probability. The only required parameters for this computation are the distance of closest approach (dist), radius of combined object (OBJ), and the ratio of major-to-minor projected covariance ellipse axes. This method begins by including the aspect ratio (AR) as a multiple of the minor axis standard deviation. Including this expression changes Equation to [8]

$$P = \frac{1}{2\pi\sigma_x^2 AR}\int_{-OBJ}^{OBJ}\int_{-\sqrt{OBJ^2-x^2}}^{\sqrt{OBJ^2-x^2}} e^{-\frac{1}{2}\left[\left(\frac{x-x_m}{\sigma_x}\right)^2+\left(\frac{y-y_m}{\sigma_x AR}\right)^2\right]} dydx$$

This method only applies for the case that the combined object does not encompass the covariance center. Given the OBJ and distance from the center, the minor axis size can be determined by maximizing a two-dimensional probability expression. Once this has been

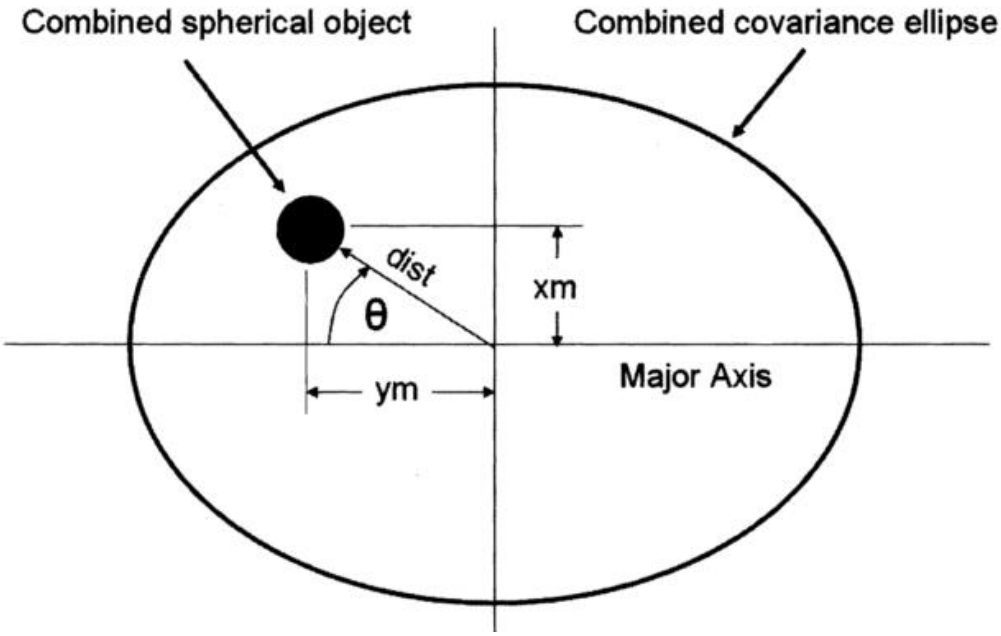

Figure 11. Modified encounter plane

determined, the worst-case collision probability is calculated. Modifying the encounter plane in Figure 10, the x_m and y_m components are varied as a function of the fixed relative distance and the angle θ. This new plane is shown below in Figure 11.

This new formulation changes Equation 8 to

$$P = \frac{1}{2\pi\sigma_x^2 AR}\int_{-OBJ}^{OBJ}\int_{-\sqrt{OBJ^2-x^2}}^{\sqrt{OBJ^2-x^2}} e^{-\frac{1}{2}\left[\left(\frac{x-(dist)\sin(\theta)}{\sigma_x}\right)^2+\left(\frac{y+(dist)\cos(\theta)}{\sigma_x AR}\right)^2\right]} dydx \quad [9]$$

The derivative with respect to θ is set to zero to find occurrences of maximum probability. This derivative will equal zero whenever θ is a multiple of π/2. The maximum probability occurs whenever θ is a multiple of π. This means then that the maximum probability occurs when the relative distance is along the major axis (x_m = 0, y_m = dist)

$$P = \frac{1}{2\pi\sigma_x^2 AR}\int_{-OBJ}^{OBJ}\int_{-\sqrt{OBJ^2-x^2}}^{\sqrt{OBJ^2-x^2}} e^{-\frac{1}{2}\left[\left(\frac{x}{\sigma_x}\right)^2+\left(\frac{y+(dist)}{\sigma_x AR}\right)^2\right]} dydx \quad [10]$$

The constant can then be pulled to the outside of the integral

$$P = \frac{e^{\frac{\left(-\frac{1}{2}\right)dist^2}{\sigma_x^2 AR^2}}}{2\pi\sigma_x^2 AR}\int_{-OBJ}^{OBJ}\int_{-\sqrt{OBJ^2-x^2}}^{\sqrt{OBJ^2-x^2}} e^{-\frac{1}{2}\left[\left(\frac{x}{\sigma_x}\right)^2+\left(\frac{y^2+2y(dist)}{\sigma_x^2 AR^2}\right)\right]} dydx \quad [11]$$

The exponential term inside is expanded to various orders and the derivative of the probability equation is taken with respect to σ_x. The resulting expression is set to zero to determine the minor axis standard deviation that maximizes probability. Dr. Alfano derives several approximate expressions for maximum probability (P_{max}) and associated minor-axis standard deviation (σ_x). These expressions are listed below.

$$\sigma x0 = \frac{dist}{\sqrt{2}AR} \quad [12]$$

$$\sigma x1 = \sqrt{\frac{(AR^2 + 1)OBJ^2 + 2dist^2 + \sqrt{[(AR^2 + 1)OBJ^2]^2 + 4dist^4}}{8AR^2}} \quad [13]$$

The second order expression σ_{x2} can be found from the expressions below.

$$\begin{gathered} a = 384AR^6 \\ b = -96[(1 + AR^2)OBJ^2 + 2dist^2]AR^4 \\ c = 6(OBJ\,AR)^2[(28 + 4AR^2)dist^2 + (3 + 3AR^4 + 2AR^2)OBJ^2] \\ d = -(dist\,OBJ)^2[(2AR^2 + 3 + 3AR^4)OBJ^2 + 24dist^2] \\ 0 = a(\sigma x2^2)^3 + b(\sigma x2^2)^2 + c(\sigma x2^2) + d \end{gathered} \quad [14]$$

The associated 3rd-order polynomial is then solved for σ_{x2}^2 and the complex numbers are discarded. The positive roots remaining are tested for maximum probability.

$$Pmax0 = \frac{OBJ^2}{2[AR(\sigma x_{Pmax})^2]} \exp\left[\frac{-1}{2}\left[\frac{dist}{AR(\sigma x_{Pmax})}\right]^2\right] \quad [15]$$

$$Pmax1 = \frac{OBJ^2}{16[AR^3(\sigma x_{Pmax})^4]} \exp\left[\frac{-1}{2}\left[\frac{dist}{AR(\sigma x_{Pmax})}\right]^2\right] [(-AR^2 - 1)OBJ^2 + 8AR^2(\sigma x_{Pmax})^2] \quad [16]$$

$$\begin{gathered} aa2 = 192AR^4(\sigma x_{Pmax})^4 \\ bb2 = (-24AR^4OBJ^2 - 24OBJ^2AR^2)(\sigma x_{Pmax})^2 \\ cc2 = (3AR^4 + 2AR^2 + 3)OBJ^4 + 24dist^2OBJ^2 \end{gathered}$$

$$Pmax2 = \frac{OBJ^2}{384[AR^5(\sigma x_{Pmax})^6]} \exp\left[\frac{-1}{2}\left[\frac{dist}{AR(\sigma x_{Pmax})}\right]^2\right](aa2 + bb2 + cc2) \quad [17]$$

$$aa3 = -3072AR^6(\sigma x_{Pmax})^6$$

$$bb3 = [(384AR^4 + 384AR^6)OBJ^2](\sigma x_{Pmax})^4$$

$$cc3 = [(-32AR^4 - 48AR^2 - 48AR^6)OBJ^4 - 384dist^2OBJ^2AR^2](\sigma x_{Pmax})^2$$

$$dd3 = (3AR^4 + 5 + 3AR^2 + 5AR^6)OBJ^6 + (96dist^2 + 32dist^2AR^2)OBJ^4$$

$$Pmax3 = \frac{OBJ^2}{6144[AR^7(\sigma x_{Pmax})^8]} \exp\left[\frac{-1}{2}\left[\frac{dist}{AR(\sigma x_{Pmax})}\right]^2\right] \quad [18]$$
$$(aa3 + bb3 + cc3 + dd3)$$

$$aa4 = 245760(AR\sigma x_{Pmax})^8 + [-30720OBJ^2(AR^2 + 1)](\sigma x_{Pmax}AR)^6$$

$$bb4 = 1280[OBJAR^2(\sigma x_{Pmax})^2]^2[(3AR^4 + 3 + 2AR^2)OBJ^2 + 24dist^2]$$

$$cc4 = -80(OBJ^2AR\sigma x_{Pmax})^2[(96 + 32AR^2)dist^2 + (5AR^6 + 3AR^2 + 5 + 3AR^4)OBJ^2]$$

$$dd4 = (35AR^8 + 35 + 20AR^6 + 18AR^4 + 20AR^2)OBJ^8 + [(1200 + 480AR^2 + 240AR^4)dist^2]OBJ^6 + 1280dist^4OBJ^4$$

$$Pmax4 = \frac{1}{491520[AR^9(\sigma x_{Pmax})^{10}]} \exp\left[\frac{-1}{2}\left[\frac{dist}{AR(\sigma x_{Pmax})}\right]^2\right] \quad [19]$$
$$OBJ^2(aa4 + bb4 + cc4 + dd4)$$

Dr. Alfano also derived the maximum percent error of the approximations listed above. Those errors are presented below in Table 4 [42].

Table 4. Maximum percent error for approximations

	$Pmax < 0.01$	$Pmax < 0.001$
$Pmax0(\sigma x0)$	35.00	3.50000
$Pmax1(\sigma x0)$	18.00	0.15000
$Pmax2(\sigma x0)$	2.00	0.05000
$Pmax3(\sigma x0)$	4.70	0.05000
$Pmax4(\sigma x0)$	2.90	0.05000
$Pmax0(\sigma x1)$	24.00	3.00000
$Pmax1(\sigma x1)$	8.00	0.13000
$Pmax2(\sigma x1)$	0.31	0.00250
$Pmax3(\sigma x1)$	1.60	0.00040
$Pmax4(\sigma x1)$	1.20	0.00032
$Pmax0(\sigma x2)$	33.00	3.00000
$Pmax1(\sigma x2)$	12.00	0.13000
$Pmax2(\sigma x2)$	2.90	0.00250
$Pmax3(\sigma x2)$	1.30	0.00006
$Pmax4(\sigma x2)$	0.32	0.00005

The maximum probability method is the model of choice in the Satellite Orbital Conjunction Reports Assessing Threatening Encounters in Space (SOCRATES) program used by the Center for Space Standards and Innovation (CSSI) [43].

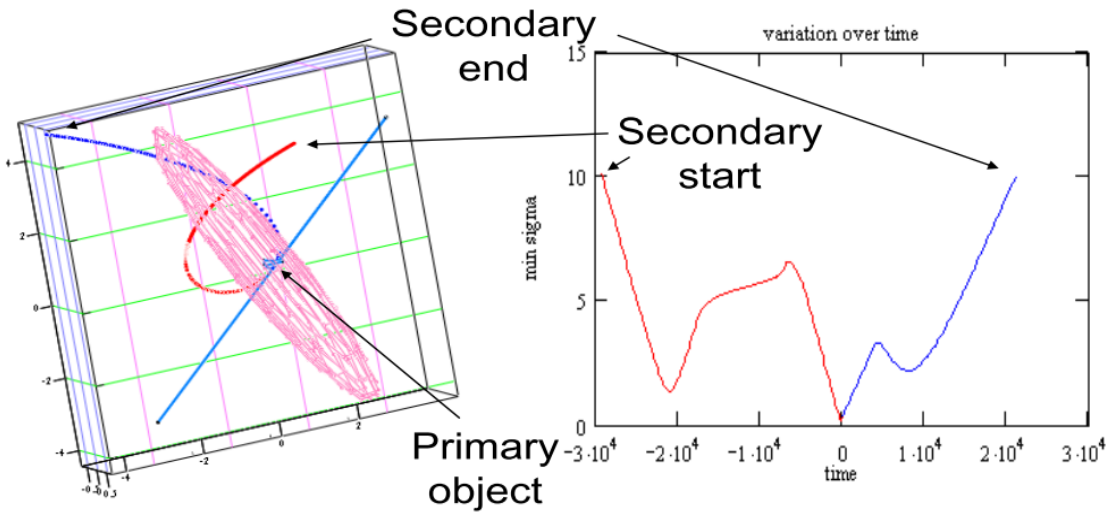

Figure 12. An example close approach where the linear relative motion assumption does not apply

Nonlinear Probability Models

For long-term close approach instances, assuming linear motion will almost certainly be an invalid assumption. These types of instances can look something like Figure 12**Error! Reference source not found.** above from Salvatore Alfano's paper ddressing nonlinear relative motion [44]. As stated previously, these types of instances typically occur in GEO and will not be directly addressed in this research.

2.7 Summary

This chapter began with a general overview of space debris, including a discussion on basics of space debris, the policy governing debris generation, and concluded with a discussion on what the future environment might look like. Following this section, the characteristics of a debris field were presented. This showed the evolution of the field from the initial belt-like look to the final debris shell. Next, there was a brief discussion on the consequences of maneuvering and the difficulty in

accurately propagating spacecraft position over time. Finally, the chapter concluded with a presentation of the leading collision likelihood models.

III. Methodology

3.1 Chapter Overview

This chapter will provide the methodology taken to approach the hypothesis, address the research objectives, and answer the posed research questions. The impetus that drove this methodology was a simulation of the Chinese ASAT test produced by Analytical Graphics, Inc (AGI). In the video, the AGI team simulated the on-orbit breakup utilizing STK. Accompanying this video was a report detailing a methodology for producing on-orbit breakup scenarios in STK [8]. Beginning with their methodology, this research makes use of the HPC, Thunder, to lessen computational burden and increase the scope. Additionally, this research uses the NASA EVOLVE 4.0 breakup model to characterize the debris and expands further to include a close approach analysis to understand the danger posed by such a hypothetical breakup.

This methodology allows for user-defined debris fields to be created at a desired location and analyzed for risk with relative ease. Additionally, the user can modify the scope of the debris field in terms of number of pieces and minimum/maximum diameters. This research demonstrates simulation and analysis of a breakup at a particular altitude (850 km) and inclination (83°), but can be modified to account for any desired location.

As previously stated, the goal of this research is to take first steps towards an operations plan for responding to an on-orbit breakup. Given a known altitude, inclination, and cause of failure, the operator will have some reference as to the danger in the immediate aftermath of a breakup. If an operator finds themselves in a danger zone, an approximate maneuver cost to get to the nearest safe zone could then be calculated.

Immediate aftermath in this context refers to a timeframe ranging from breakup occurrence to one week in the future. One week was chosen as it falls into the time window where the debris has not been cataloged and thus much is unknown.

Section 3.2 describes the general 3-step methodology for the research. Section 3.3 describes the code itself and how the HPC is utilized to reduce the computational time for such a large scenario. Finally, Section 3.4 describes the data analysis techniques and metrics used to analyze the results.

3.2 General Methodology

The general process works in three steps: modifying the python debris code, submitting the job on the supercomputer, and parsing the data. These steps are described in detail below:

Step 1 – Python Debris Code

In this step, the user defines the debris field characteristics. The number of debris pieces is governed by NASA's EVOLVE 4.0 breakup model. The breakup is simulated through applying an impulsive thrust one second after the initial state is propagated. This thrust vector is in spherical coordinates with azimuth, elevation, and velocity magnitude components. The azimuth and elevation are both pulled from a normal distribution centered at 0 degrees with a standard deviation of 30 degrees. These values were chosen as they were the same used by Carrico et al. in *Investigating Orbital Debris Events Using Numerical Methods with Full Force Model Orbit Propagation* [8]. The velocity magnitude component values are pulled from the distribution created in the NASA EVOLVE model. The NASA EVOLVE Model was chosen as it provided the ability to

rapidly model the explosion. The generated debris field will be analyzed by the ACAT for close approaches against STK's all TLE file. This TLE file contains all catalogued on-orbit objects, both active and inactive. The ACAT uses threat volumes around the satellite as a rough estimate of covariance to analyze close approaches and compute probability of collision. A threat sphere of one kilometer in all directions was chosen for all scenario objects (debris pieces and TLE objects). This was chosen as it is the current warning volume used by JSpOC for collision likelihood warnings. A collision warning will be issued if one threat sphere comes within one kilometer of another threat sphere, meaning the maximum possible range in an encounter is three kilometers (threat radius of object + threat distance + threat radius of debris).

The code will output several pre-defined reports that will later be parsed. It is currently set to produce reports that contain the necessary information to create a Gabbard plot, view the classical elements of the debris, view the close approaches within a certain distance threshold, and analyze the probabilities of collision from several models. The Gabbard and classical element reports were chosen because they give enough information to accurately statistically characterize the debris field. The last two report types (close approach and probability of collision) were chosen as they provide the number of encounters, distances of encounter, and associated probability of collision. The combination of all reports will satisfy the desired research objectives. The user can create their own additional reports as desired, but this requires modification of both the primary and parsing scripts.

NASA EVOLVE Breakup Model 4.0

The NASA EVOLVE breakup model is used to define the size, area-to-mass ratio, and ejection velocity of each of the debris fragments. This model was chosen at it is one of the most popular models currently being used. It also allows for rapid generation of the attributes necessary to define the debris pieces. The model can be used for either explosions or collisions. This research only utilizes the explosion portion of the model. Equation 20 below is used to calculate the number of fragments of size L_c or larger.

$$N(L_c) = S6L_c^{-1.6} \quad [20]$$

- Lc = characteristic length (diameter) in meters
- S = unitless scale factor (more details on this factor found in [45])

The 4th installment of the EVOLVE model bases its area-to-mass distributions on extensive analysis of fragmentation debris cataloged by the Space Surveillance Network. For area-to-mass values less than one m^2/kg, this method has proven to be a good approximation of the actual average area-to-mass. For values greater than one m^2/kg, this approximation leads to possible issues with mass calculations but is still good for computing orbital lifetime. The distribution function for spacecraft fragments with L_c larger than 11 centimeters is given by Equation 21 below.

$$D_{A/M}^{S/C}(\lambda_c,\chi) = \alpha^{S/C}(\lambda_c)N(\mu_1^{S/C}(\lambda_c), \sigma_1^{S/C}(\lambda_c),\chi) + (1 - \alpha^{S/C}(\lambda_c))N(\mu_2^{S/C}(\lambda_c), \sigma_2^{S/C}(\lambda_c),\chi) \quad [21]$$

where

$\lambda_c = \log_{10}(L_c)$

$\chi = \log_{10}(A/M)$ is the variable in the distribution

N = the normal distribution function: $N(\mu,\sigma,\chi) = [1 / \sigma(2\pi)^{0.5})]\, e^{-(\chi-\mu)2 / 2\sigma 2}$

and

$$\alpha^{s/c} = \begin{cases} 0 & \lambda_c \le -1.95 \\ 0.3 + 0.4(\lambda_c + 1.2) & 1.95 < \lambda_c < 0.55 \\ 1 & \lambda_c \ge 0.55 \end{cases}$$

$$\mu_1^{s/c} = \begin{cases} -0.6 & \lambda_c \le -1.1 \\ -0.6 - 0.318(\lambda_c + 1.1) & -1.1 < \lambda_c < 0 \\ -0.95 & \lambda_c \ge 0 \end{cases}$$

$$\sigma_1^{s/c} = \begin{cases} 0.1 & \lambda_c \le -1.3 \\ 0.1 + 0.2(\lambda_c + 1.3) & -1.3 < \lambda_c < -0.3 \\ 0.3 & \lambda_c \ge -0.3 \end{cases}$$

$$\mu_2^{s/c} = \begin{cases} -1.2 & \lambda_c \le -0.7 \\ -1.2 - 1.333(\lambda_c + 0.7) & -0.7 < \lambda_c < -0.1 \\ -2.0 & \lambda_c \ge -0.1 \end{cases}$$

$$\sigma_2^{s/c} = \begin{cases} 0.5 & \lambda_c \le -0.5 \\ 0.5 - (\lambda_c + 0.5) & -0.5 < \lambda_c < -0.3 \\ 0.3 & \lambda_c \ge -0.3 \end{cases}$$

For fragments with Lc smaller than 8 centimeters, the area-to-mass distribution is given by Equation 22 below.

$$D_{A/M}^{SOC}(\lambda_c,\chi) = N(\mu^{SOC}(\lambda_c), \sigma^{SOC}(\lambda_c),\chi) \qquad [22]$$

where

$$\mu^{soc} = \begin{cases} -0.3 & \lambda_c \le -1.75 \\ -0.3 - 1.4(\lambda_c + 1.75) & -1.75 < \lambda_c < -1.25 \\ -1.0 & \lambda_c \ge -1.25 \end{cases}$$

$$\sigma^{soc} = \begin{cases} 0.2 & \lambda_c \le -3.5 \\ 0.2 + 0.1333(\lambda_c + 3.5) & \lambda_c > -3.5 \end{cases}$$

To bridge the gap between 8 centimeters and 11 centimeters, a random number, ζ_d, is generated between zero and one and is compared with the value of ζ given by Equation 23 below.

$$\zeta = 10(log_{10}(L_c) + 1.05) \quad [23]$$

If $\zeta_d > \zeta$, Equation 21 for fragments greater than 11 centimeters will be used. Otherwise, Equation 22 for fragments less than 8 centimeters will be used [46]. The average cross-sectional area of the pieces is calculated via Equations 24 and 25 below.

$$A = 0.540424 L_c^2 \qquad where\ L_c < 0.00167\ meters \quad [24]$$

$$A = 0.556945 L_c^{2.0047077} \qquad where\ L_c \ge 0.00167\ meters \quad [25]$$

This leaves the task of converting the values thus far to mass via Equation 26 below.

$$M = \frac{A}{\frac{A}{M}} \quad [26]$$

The final portion of the NASA EVOLVE Model will derive the ejection velocity for the pieces. This section utilizes area-to-mass as the independent variable instead of the diameter that has been utilized thus far. The ejection velocity distribution is found in Equation 27 below.

$$D_{\Delta v}^{EXP}(\chi, v) = N(\mu^{EXP}(\chi), \sigma^{EXP}(\chi), v) \quad [27]$$

where

$$\chi = \log_{10}(A/M)$$
$$\nu = \log_{10}(\Delta V)$$
$$\mu^{EXP} = \text{mean} \approx 0.2\chi + 1.85$$
$$\sigma^{EXP} = \text{standard deviation} = 0.4$$

The variables derived above are then input into the debris objects defined within STK [45], [47].

Step 2 – Run on Supercomputer

Once the field has been characterized in the python script, the job can be submitted into the supercomputer que via a PBS script. This requires getting a ticket for the supercomputer via the Kerberos application and then logging in via the PuTTY application. A full description of the methodology for signing into the supercomputer can be found in the Thunder User Guide [48]. The supercomputer being used for this research is the Air Force Research Lab (AFRL) Defense Supercomputing Resource Center (DSRC) computer, *Thunder*. *Thunder* is an SGI ICE X system rated for 5.62 peak PFLOPS. The standard memory section used for this research contain 3,216 nodes with 36 cores per node for a grand total of 115,776 nodes. Additionally, there are 128 GBytes of memory in each node [48]. A full description of the *Thunder* computer can be found in the appendices. Successful submission of a job will look like Figure 13 below.

```
thunder05:/home/dbuehler/Working/Project/ python buehlsCAT-debPBS.py
l:ncpus=36:mpiprocs=4
thunder05:/home/dbuehler/Working/Project/ 1471941.thunder-b01
```

Figure 13. Job submission for supercomputer. number of nodes requested is 1, 36 is the number of CPUs per node, and 4 is the number of processes per node.

A job that is running will look like Figure 14 below.

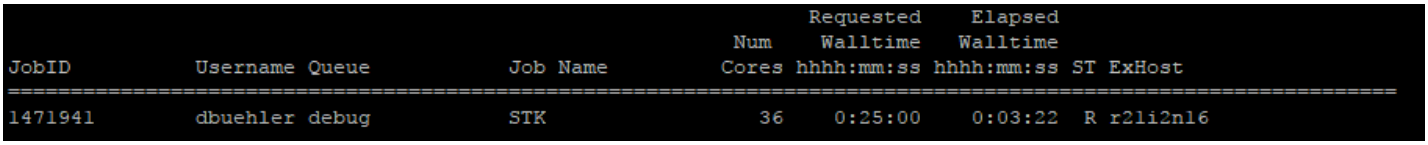

Figure 14. Running job on the supercomputer

Upon completion of the job, the reports from the STK scenario are saved to the working directory and are ready for parsing.

Step 3 – Parse Results

A successful run will result in data reports that need to be parsed, recombined, visualized, etc. With the size of the debris fields being 100,000 pieces or more, there is a substantial amount of data to sort through. With four Gabbard/COE reports per debris piece, two close approach and probability reports per ACAT, and five characteristic reports per scenario, the code generates over 400,000 reports in one run of 100,000 pieces. Doing this one report at a time is simply not an option. Another python script is utilized to parse the reports. The script will look for the report location and step through each report, gleaning data as it goes. It then combines all the gathered data into one large .csv file that can be visualized. Custom report styles can be created in the STK Graphical User Interface (GUI) and uploaded to the supercomputer. This allows the user to add and subtract information as necessary. Parsing a file that only includes needed information is much easier than having to step through unnecessary information. Full instruction on how to create, save, and upload custom reports can be found in the appendices. The activity of the three-step process is visualized in Figure 15 on the following page.

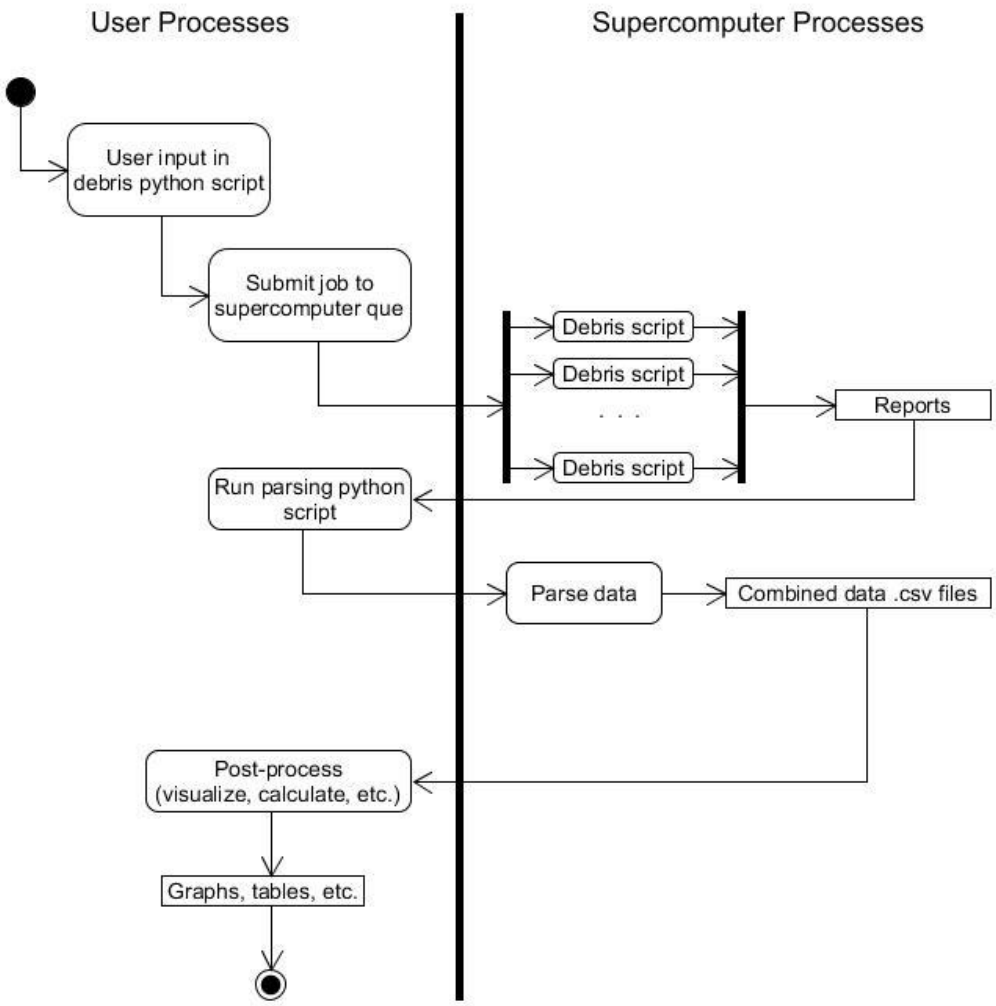

Figure 15. Activity diagram for breakup simulation

3.3 Code Breakdown

As stated previously, the code works in two parts: one code string that runs the scenario and outputs reports and another string that parses those reports. The supercomputer reduces the computational burden and time because it allows for parallelization of STK. Rather than run either one 100,000-piece scenario or 500, 200-

piece scenarios one after the other, one can simply run 500, 200-piece scenarios in parallel.

The only downside to running STK on the supercomputer is the loss of the program's excellent visualization. The supercomputer is designed to be as efficient as possible, this means visualization is simply not an option. To give an idea of what the debris scenario looks like within STK, Figure 16 below is the breakup code visualized with 250 pieces (red) run against the catalog of known objects (green).

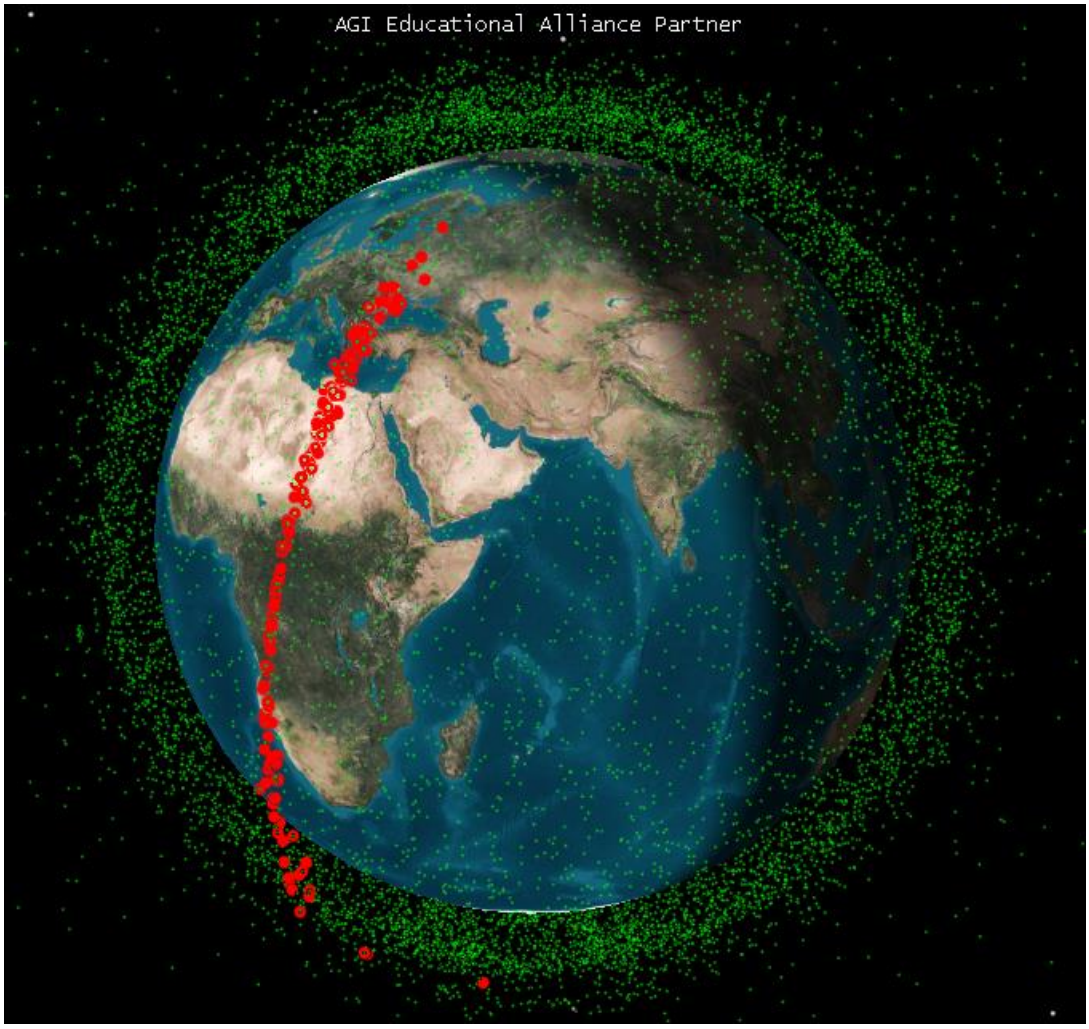

Figure 16. 250-piece breakup scenario visualization

The top of the scenario code can be altered to account for a number of different initial conditions for the breakup. These initial conditions are then processed through the STK scenario and reports with data to characterize the debris and close approaches are output.

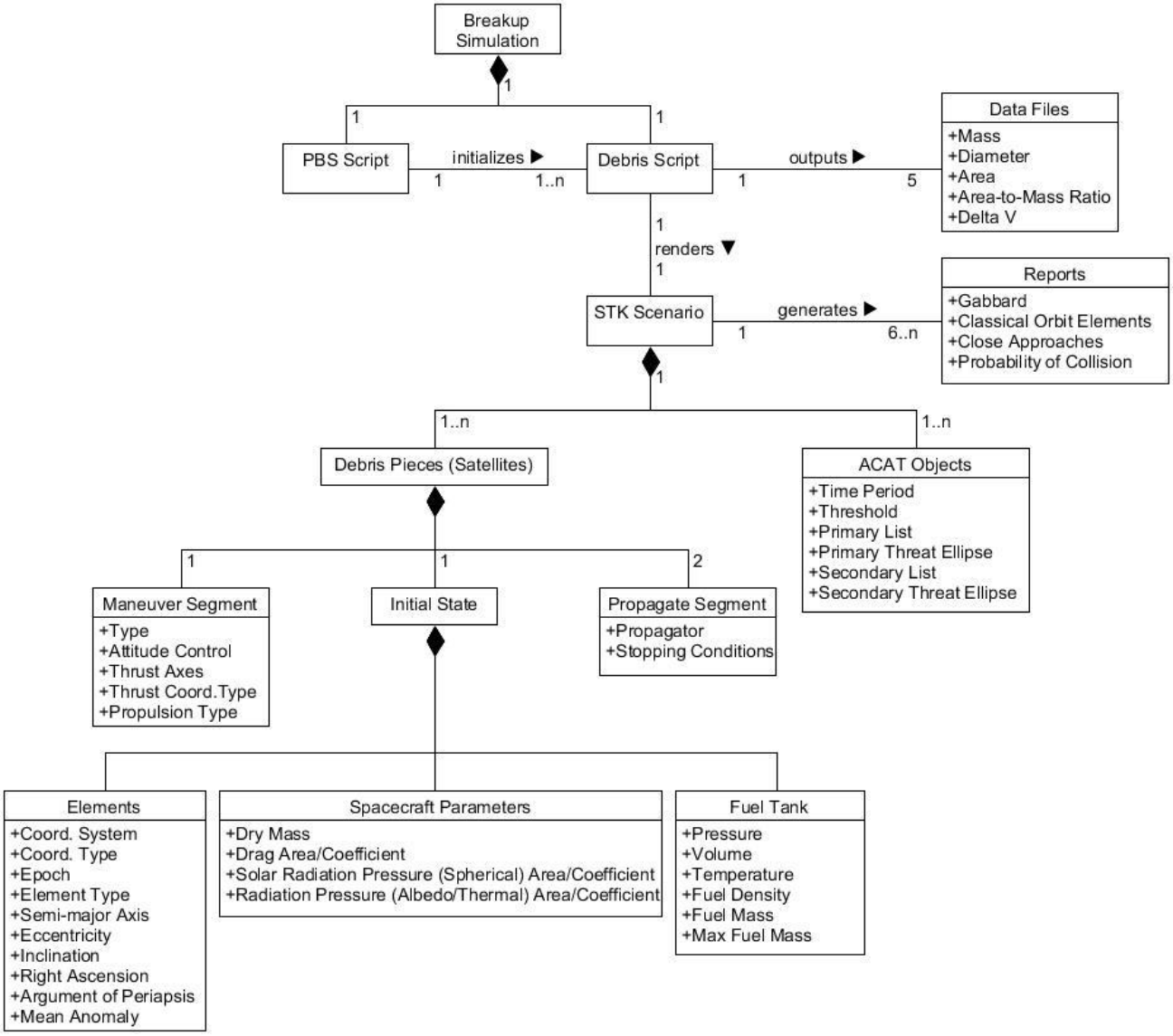

Figure 17. UML class diagram of research methodology

Figure 17 above is a unified modeling language (UML) class diagram that summarizes the methodology nicely. The Gabbard and COE reports output by the scenario are ~60 bytes and ~80 bytes respectively. The Close Approach and Probability of Collision reports are larger at ~20 KB each and the 7,000 reports over one week of analysis brings the total data generated for 100,000 pieces with seven ACATs to ~180 MB. This value will vary based on number of pieces, number of close approach tool objects, propagation time, etc.

3.4 Data Analysis Techniques

The Gabbard reports contain the information to make a Gabbard plot. The Gabbard plot was invented by a NORAD employee named John Gabbard in the 1960-70's. It is used to show the relative location of debris pieces from breakup events. It plots the orbit period on the x axis and the pair of apogee and perigee altitudes of each debris piece on the y axis. Objects to the left of the breakup point have lower periods and are most likely to reenter next. An example of this type of plot is shown below in Figure 18 [49].

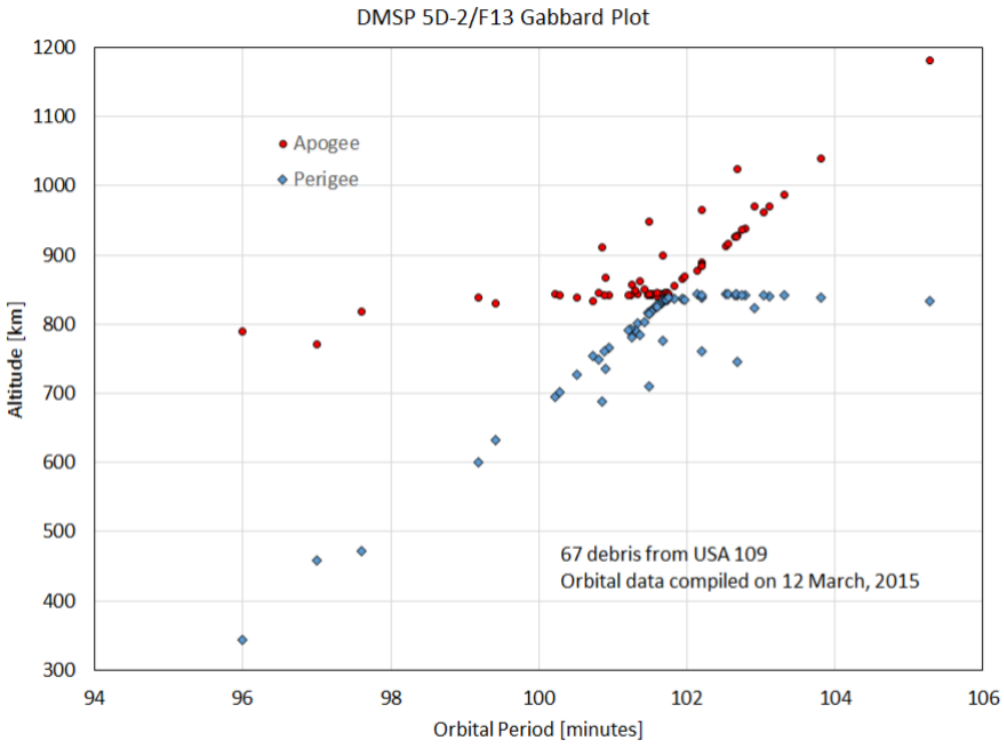

Figure 18. Gabbard plot for DMSP 5D-2/F13

In addition to the above plot, a modified Gabbard plot will be utilized. The modified Gabbard plot will simply replace period with inclination on the x axis. This will give insight into the spread of affected orbital inclinations.

The Close Approach reports will be used to record the quantity of close approaches per day for the weeklong scenario. These reports cross-reference the generated debris with the catalog of on-orbit objects and detail the number of close approaches within a user-defined threshold. Coupling this report with the Combined Collision Probability report quantifies the risk with each of these close approach events. This report contains probabilities calculated via the following models previously-discussed in Chapter 2.6:

- Salvatore Alfano’s Numeric Method
- Russell Patera’s 2005 Method
- Ken Chan’s Analytic Method
- Salvatore Alfano’s Maximum Likelihood Method

IV. Analysis and Results

4.1 Chapter Overview

The purpose of this chapter is to present the results of the debris simulation methodology described in Chapter 3. This chapter will also present the answers to research questions posed in Chapter 1. Section 4.2 presents the results of the characterization of the debris field. Section 4.3 will be a discussion of the ACAT results. In this section, the amount of close approaches and probability of collision calculated by the various models will be presented.

4.2 Debris Field Characterization

This section will discuss the results of the characterization of the debris field itself. This will include a discussion of the Gabbard plots generated by the scenarios, time for the pieces to reenter, and the nodal precession rate.

Gabbard Plots

Gabbard plots for the field were initially planned to be generated on a daily basis. This idea was abandoned as it resulted in several hundred thousand extra reports and five extra plots with relatively little insight gained. The decision was made to simply collect Gabbard data on the first day of the week and on the last day. This would allow for insight into the spread of the field, while minimizing the report storage footprint. Figure 19 and Figure 20 below are the Gabbard plots for the field for day one and day seven respectively.

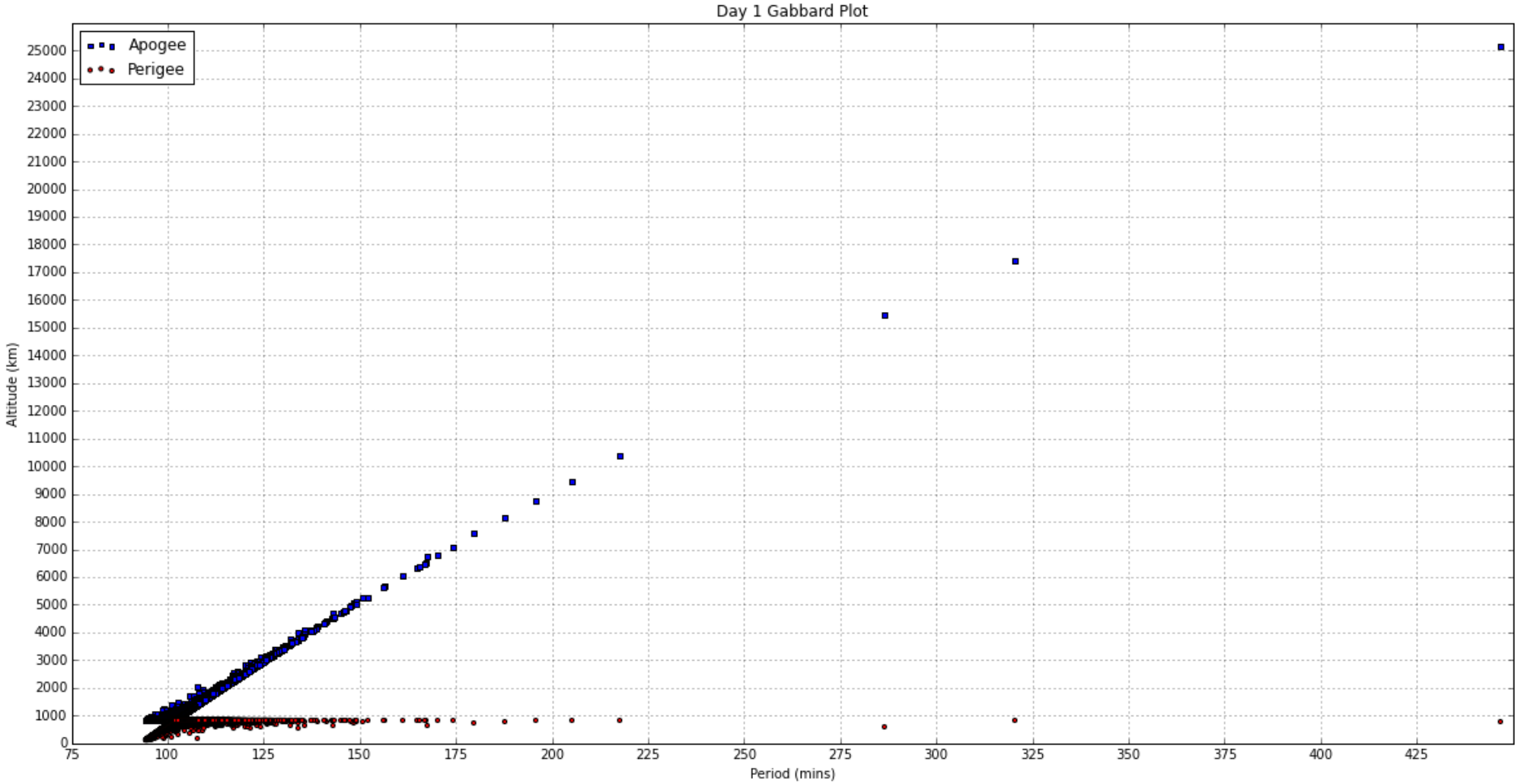

Figure 19. Gabbard plot for Day 1 data

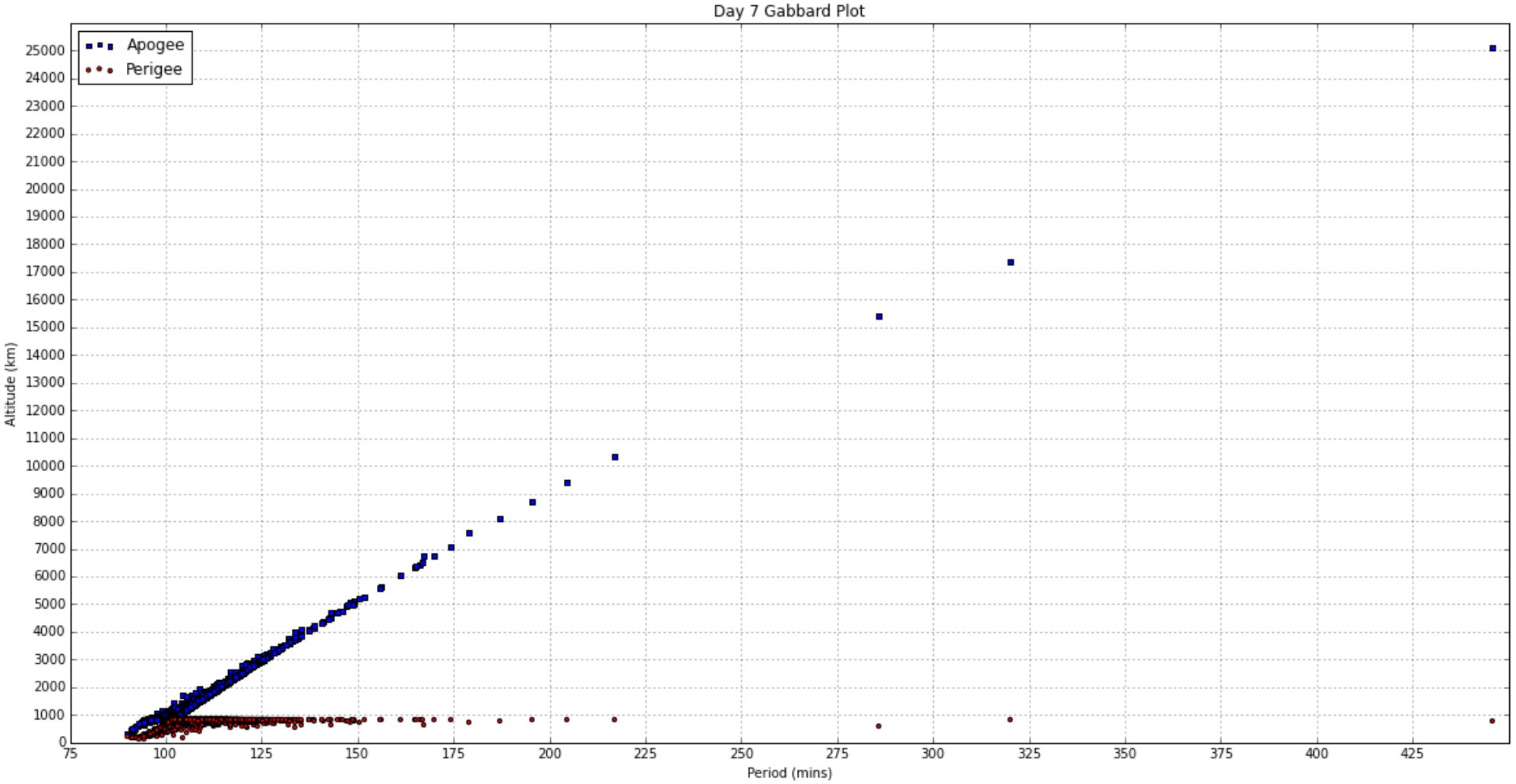

Figure 20. Gabbard plot for Day 7 data

From the plots, there are some clear outliers evident at first glance. The explanation for many of these outliers lies in the way that the parameters are pulled from the NASA EVOLVE model. Since the model pulls many of the values from a normal distribution, there is always the likelihood, albeit small, of having something beyond 3σ. Viewing the data for the furthest outlying point reveals that the suspicion is confirmed. That particular piece had a 2.3 km/s velocity imparted on it, while the average Δv for the entire scenario was 65 m/s. This, coupled with the fact that the imparted velocity has a chance of being roughly in the same direction as the initial velocity vector, can lead to a piece entering a highly elliptical orbit like the point in question.

Figure 21 on the following page contains the previous plots constrained to LEO pieces only (mean motion < 11.25)[50]. This shows the portion of the field that will be most likely to cause problems. The drift of the pieces over the course of the week can be clearly seen in the bottom figure. The pieces on the extreme left side of the plot are close to the reentry altitude (120 kilometers), while the pieces on the right will stay in orbit for longer. This sample of the debris field ranges from a minimum 152-kilometer perigee to a maximum 3,235-kilometer apogee. These results can be compared to the Gabbard plot of the FY-1C ASAT in Figure 22. The FY-1C breakup at the time of this sample ranged from 167-kilometer perigee to 3,921-kilometer apogee [27]. These values can be compared to show that the ASAT test was likely a higher energy event than the breakup simulated in this research. This higher energy causes significant fragmentation, meaning many small pieces that are thrown into higher apogees and lower perigees.

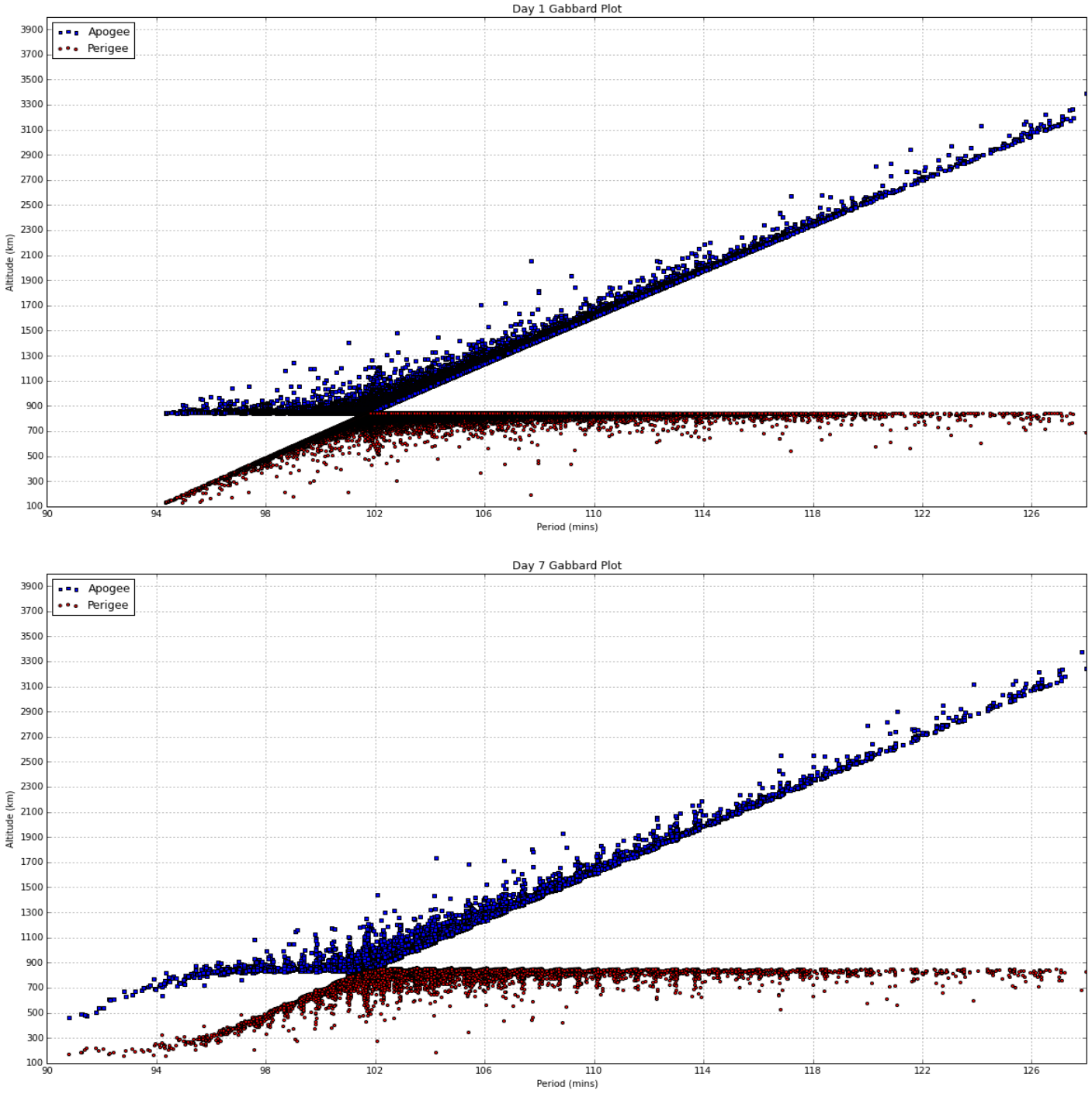

Figure 21. Gabbard plot of debris pieces within LEO period.

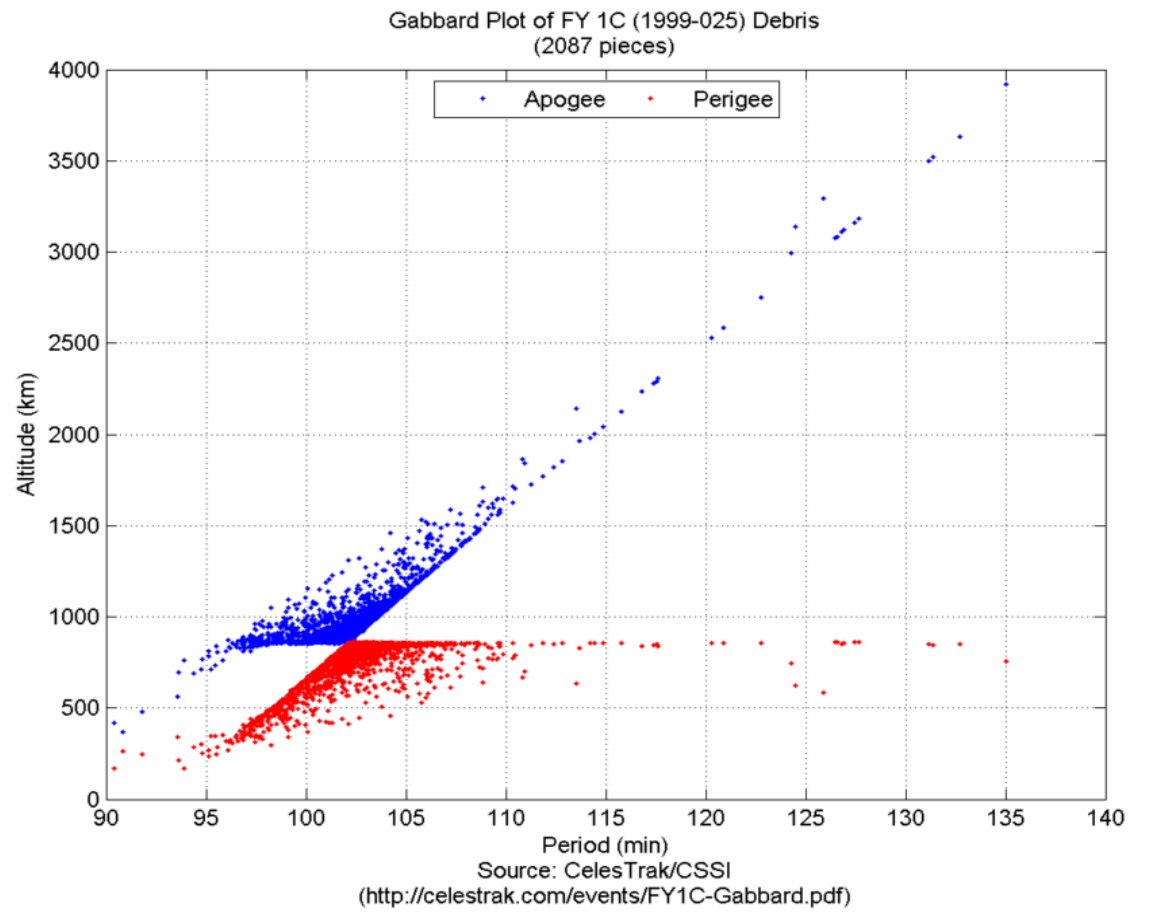

Figure 22. Gabbard plot of FY-1C ASAT test

Modified Gabbard Plots

Figure 23 on the following page is a modified Gabbard plot for the debris field. This plot is similar in that it includes the apogee/perigee pairs, but plots them against the inclination on the x axis. Only data for day seven are plotted here as the change in inclination of the objects over the course of one week was negligible (Average inclination of the cloud changes only 0.0121º over the course of one week). The day one plot can be found in the appendices for reference.

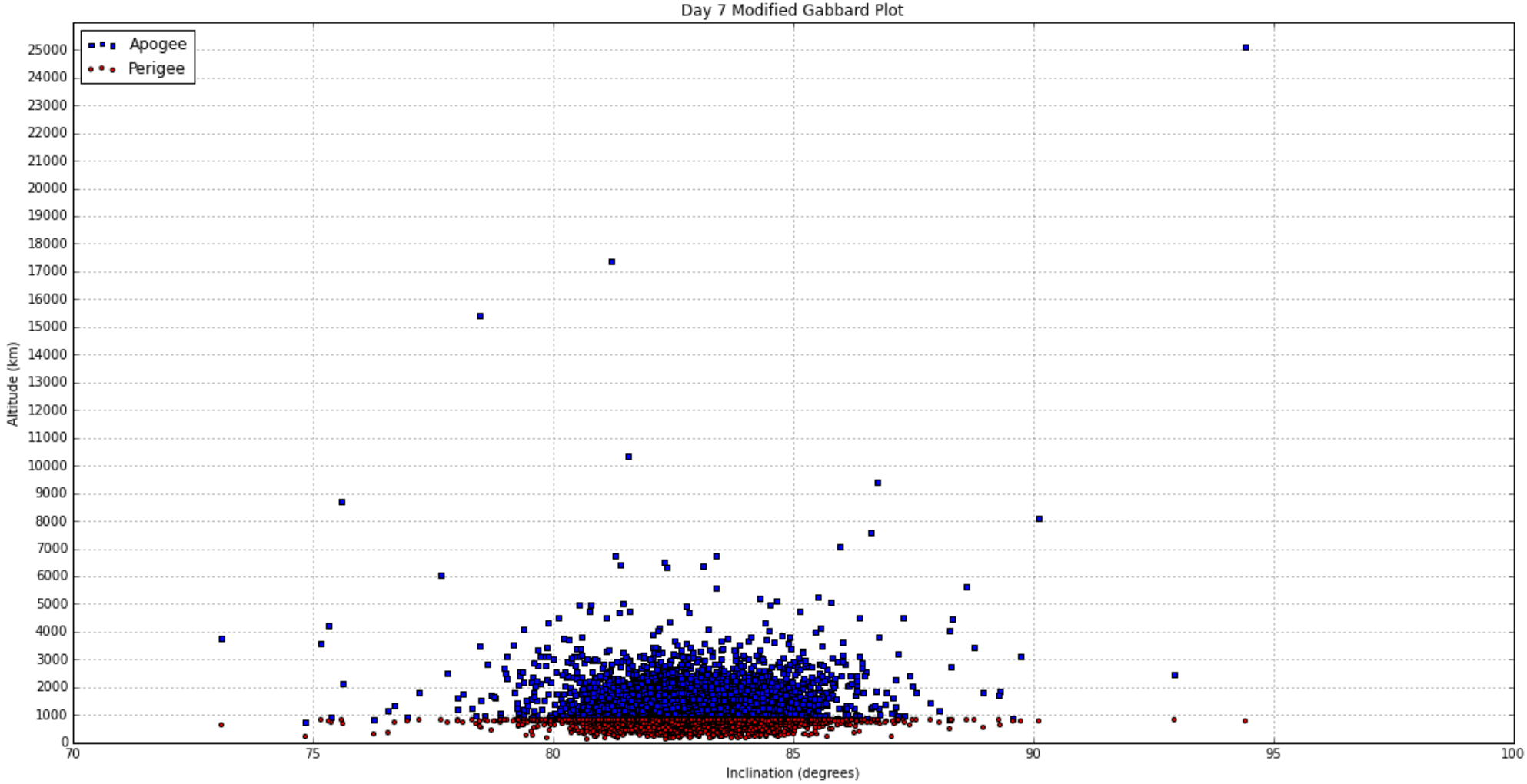

Figure 23. Modified Gabbard plot Day 7 data

The same outliers noted in the previous section stand out clearly in the top-level view. To better observe trends, this plot was reduced to the same altitude region as in the standard Gabbard plots. This can be seen in Figure 24 below. Noting the original inclination of the parent satellite at 83º, the explosion is observed to create a spread of debris that is mostly contained within approximately ± 1.5º of the original parent inclination.

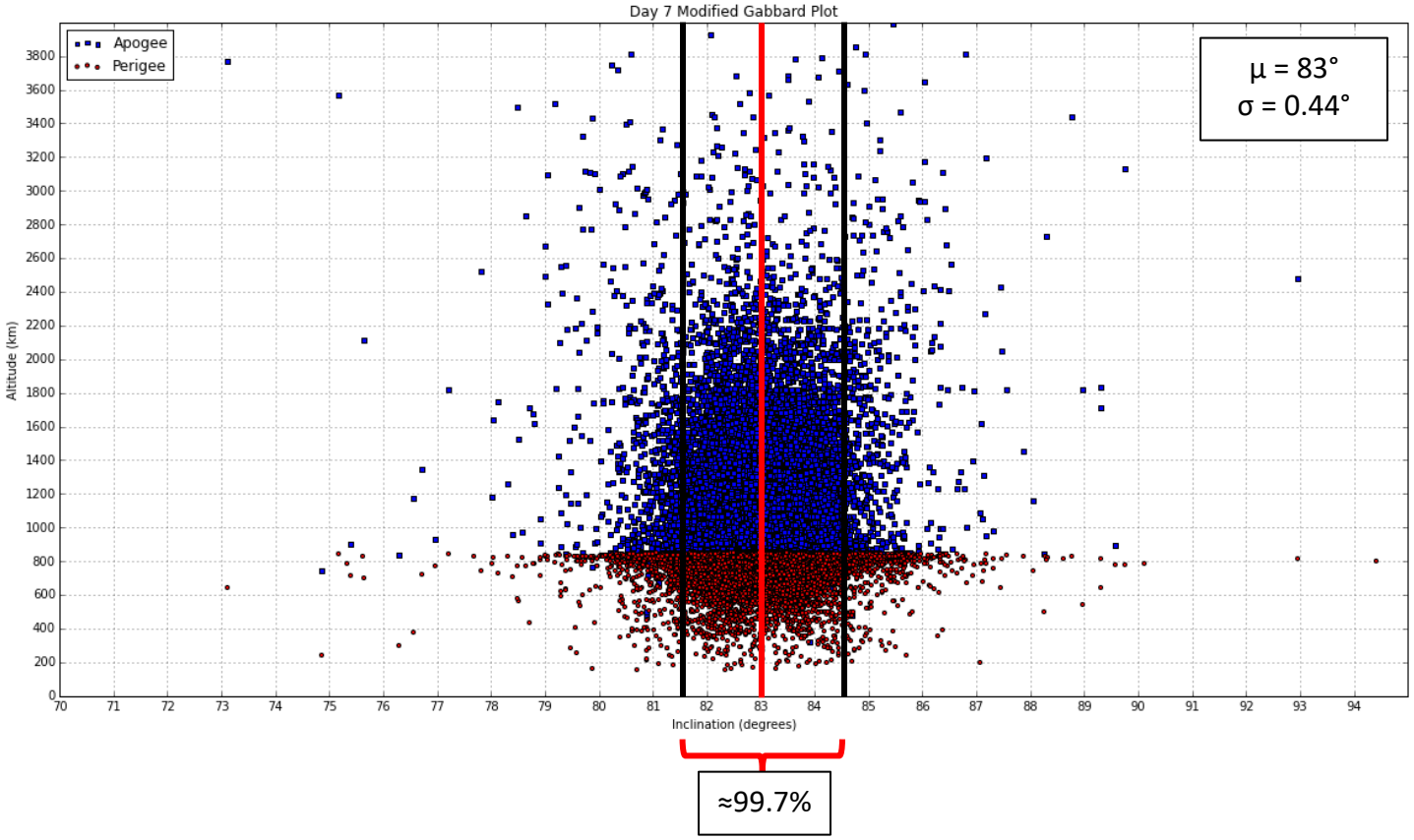

Figure 24. Modified Gabbard plot constrained to 4,000-kilometer ceiling

4.3 Debris Features

This section will discuss the characteristics of the debris pieces. The properties to be discussed are the mass, area, diameter, area-to-mass ratio, and Δv. Additionally, both the nodal precession rates and time for the pieces to decay will be calculated.

Characteristics

Table 5. Debris piece characteristic statistics

Characteristic	Units	Average	Standard Deviation	Minimum	Maximum
Area	m^2	0.1867768	0.1664155	0.0000049	0.5569450
Mass	kg	3.2753223	4.0572093	0.0000009	75.1517982
Area-to-Mass	$\frac{m^2}{kg}$	0.1154134	0.2149452	0.0005878	18.5000693
Diameter	m	0.5026981	0.2884048	0.0030000	1.0000000
Δv	$\frac{m}{s}$	65.3541450	76.6934331	0.8007466	3157.3402200

Table 5 above provides the statistics for the characteristics of the debris. All characteristics were generated within the NASA EVOLVE 4.0 model except for diameter. Diameter is user-defined and randomly pulled from a list of possible diameters ranging from three millimeters to one meter. This list is spaced in one-millimeter increments allowing for 997 possible diameters. This spacing was chosen for simplicity, but can be changed to allow for greater or fewer diameters as desired. For this exercise, the debris field was static at 100,000 pieces. This value also can be increased or decreased as desired

At first glance, the maximum values are far outside of the expected range. These values are extreme outliers in that for all characteristics, ~99.7% of the values lie within 3σ. It doesn't mean these values are impossible, just highly unlikely. For this research, the outliers were kept as there were so few and the end results were essentially unaffected by them.

Nodal Precession

The newly formed debris pieces will begin to experience the effects of Earth's oblateness. This oblateness will cause the right ascension of the ascending node (RAAN) to precess at a rate described by Equation 28 below [28].

$$\dot{\Omega} = -\frac{3nJ_2R_{\oplus}^2}{2a^2(1-e^2)^2}\cos(i) \quad [28]$$

- J_2 = 0.001082
- $R_{\oplus}$ = 6378.135 (km)
- n = mean motion (revs/day)
- a = semi-major axis (km)
- e = eccentricity
- i = inclination (deg)

The average nodal precession for this debris field is -0.76538 degrees/day. Table 6 below depicts how the node of the field moves with time. Close attention should be paid to the growth of the standard deviation, as this parameter is what truly shows the spread of the field.

Table 6. Nodal precession statistics over time

	1 Month	6 Months	1 Year	2 Years
Mean Node (degrees)	332.4371	217.6309	76.27238	203.9026
Standard Deviation of Node (degrees)	2.78396	11.01366	21.0325	40.62254

From these values, in two years, the bulk of this debris will affect a nodal range of ± 120° using 3σ. This is best shown historically by the FY-1C field in Figure 25 below.

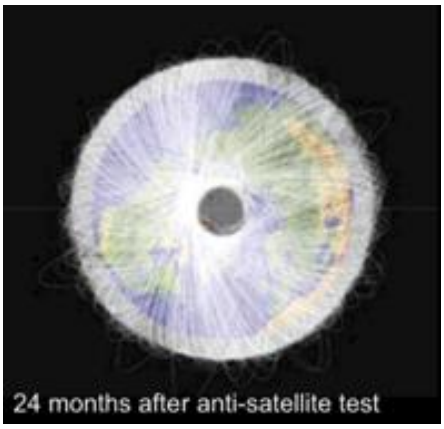

Figure 25. FY-1C debris field spread over two years

4.4 Close Approach Tool Results

This section will present the results of the close approach analysis. This first discussion will be regarding the minimum range of encounters for the week. The second half of the section will present the probability of collision for these associated minimum range encounters.

Minimum Range Results

As stated previously, the ACAT cross-references the generated debris pieces with the catalog of on-orbit objects. The scenario was run using catalog data for the week of 2 March 2017 at 0000 to 9 March 2017 at 0000. To ensure positional accuracy, a new ACAT object was created for each day of the week and referenced the historical TLE file for that day of the week. This increased the accuracy at the expense of computational time, which will be discussed later in the paper as it pertains to Research Objective #3. If an object came within three kilometers of any piece of debris in the week following the breakup it was recorded in the data file. These encounters were placed into three different bins. Within one kilometer was recorded as a "red" encounter, whereas anything between one and two kilometers was "yellow" and greater than two kilometers was deemed "green."

Over the course of one week, there were 725,165 close approaches recorded with the catalog and the debris. The weighted average of the minimum range for the passes was 2.0544 kilometers with a standard deviation of 0.0144 kilometers. Of these passes, 79,300 (~11%) were within the 1-kilometer red zone and 240,812 (~33%) were within the two-kilometer yellow zone. This is visualized through Figure 26 on the following page. Furthermore, of the red zone passes, roughly 2.5% passed within 500 meters. For reference, SOCRATES, a close approach warning system from CSSI, predicted a close approach of about 584 meters for the Iridium/Cosmos collision [51].

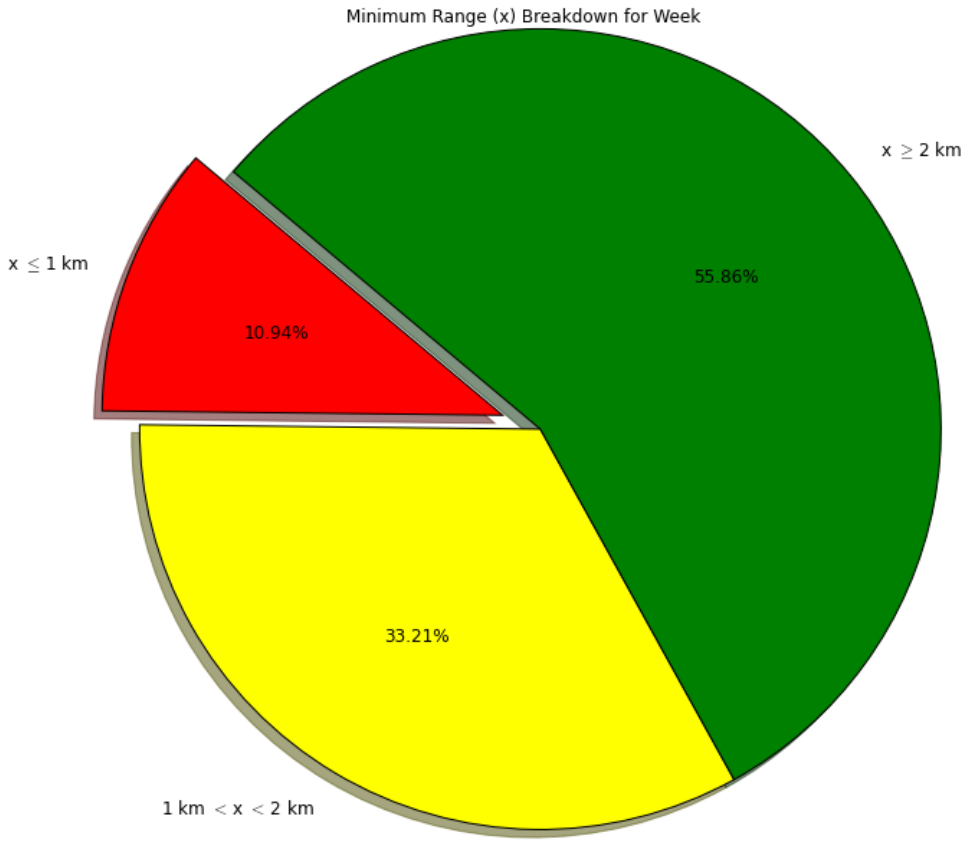

Figure 26. Top-level distribution of minimum range zones for analysis week

For a full statistical breakdown of the minimum range parameter, please refer to Figure 27 on the following page.

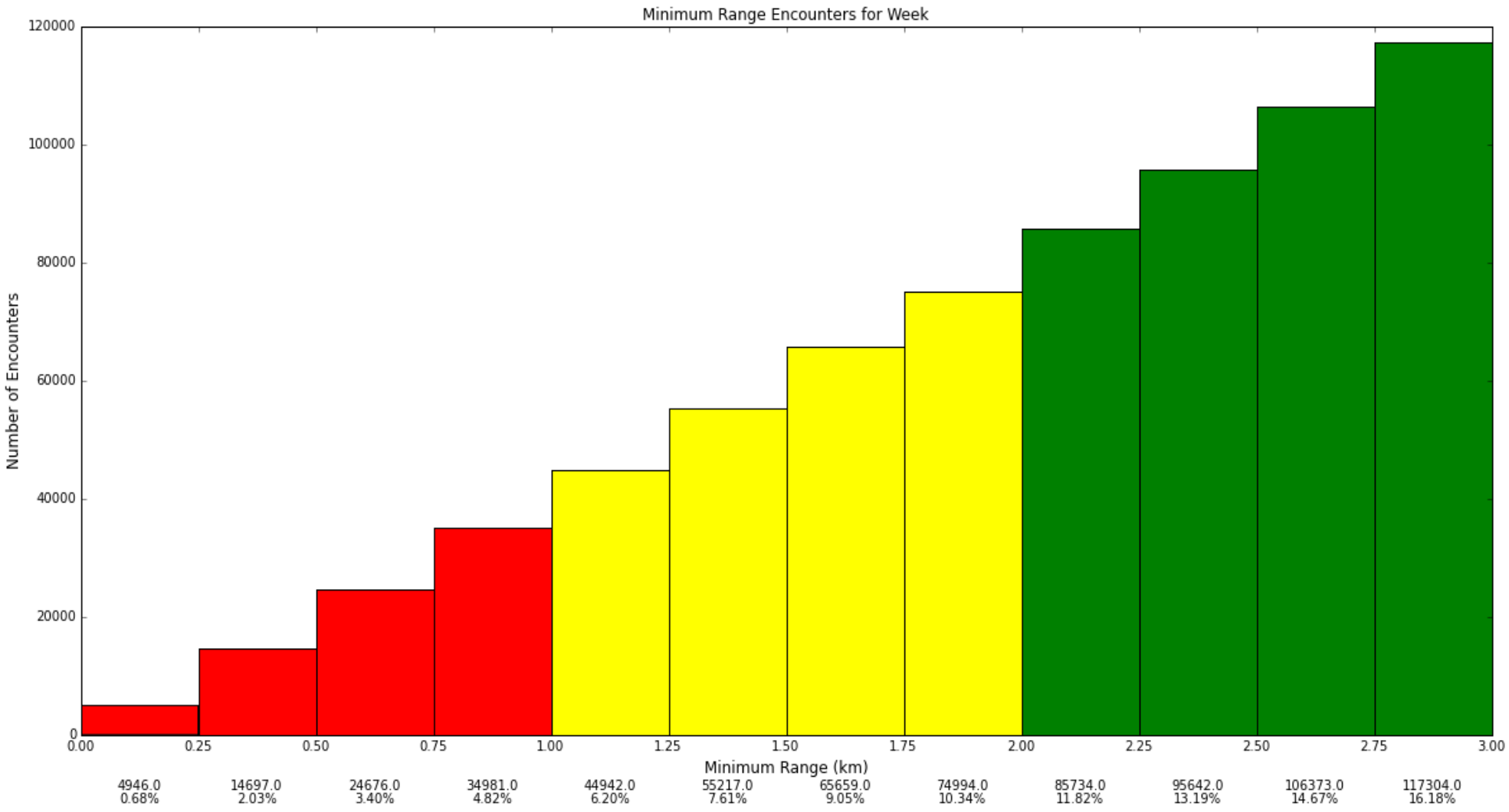

Figure 27. Histogram of minimum range encounters for analysis week

Minimum Separation Results

The next section will discuss the results of the minimum separation parameter. This parameter is the distance between the threat spheres surrounding the two objects as they pass each other. An event has occurred whenever the spheres passed each other within one kilometer. A similar approach to the minimum range section was taken in terms of dividing the events into different-colored bins. The scale here is slightly different due to the smaller maximum being at one kilometer. These bins were divided into four colors where the red zone is less than 250 meters, orange is between 250 and 500 meters, yellow is between 500 and 750 meters, and green is greater than 750 meters. The top-level breakdown can be seen in Figure 28 below.

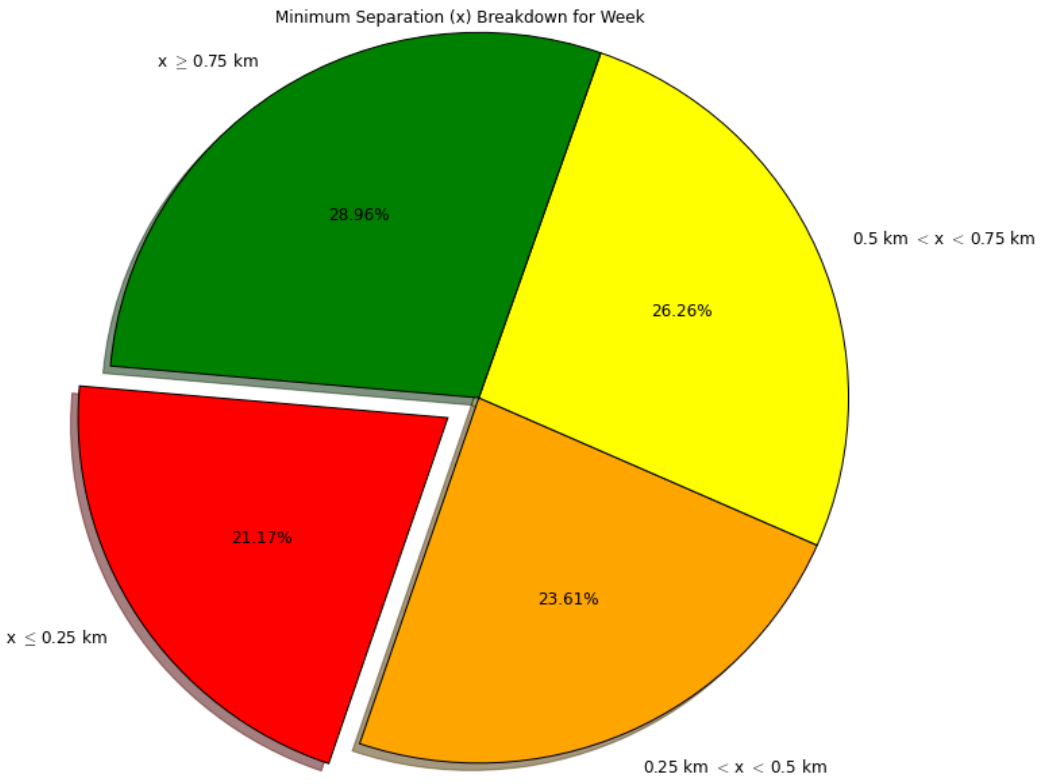

Figure 28. Top-level distribution of minimum separation zones for analysis week

Since the sphere defined by the user is supposed to be somewhat of a measure of positional covariance, it is important to note the minimum separation values. The range measure assumes the satellite is at the center of its sphere, whereas this is not likely as the satellite could be anywhere within the sphere. A much larger red zone can be noted for this breakdown. For a worst-case scenario, where both the satellite and debris were on the edge of their spheres, the range would be approximately one kilometer smaller than recorded by the minimum range measurement. This turns the values that are recorded as yellow zones into red zones, and the green zones into yellow zones. This is just to highlight the importance of noting the possibility that the ranges could be much closer than those reported by the ACAT.

The weighted average of the minimum separation parameter was found to be 0.5346 kilometers with a standard deviation of 0.01 kilometers. Of further note is that approximately 10% of the close approach encounters involved spheres that passed within 125 meters of each other. As with the minimum range measure, a full breakdown of the minimum separation measure can be found in Figure 29 on the following page.

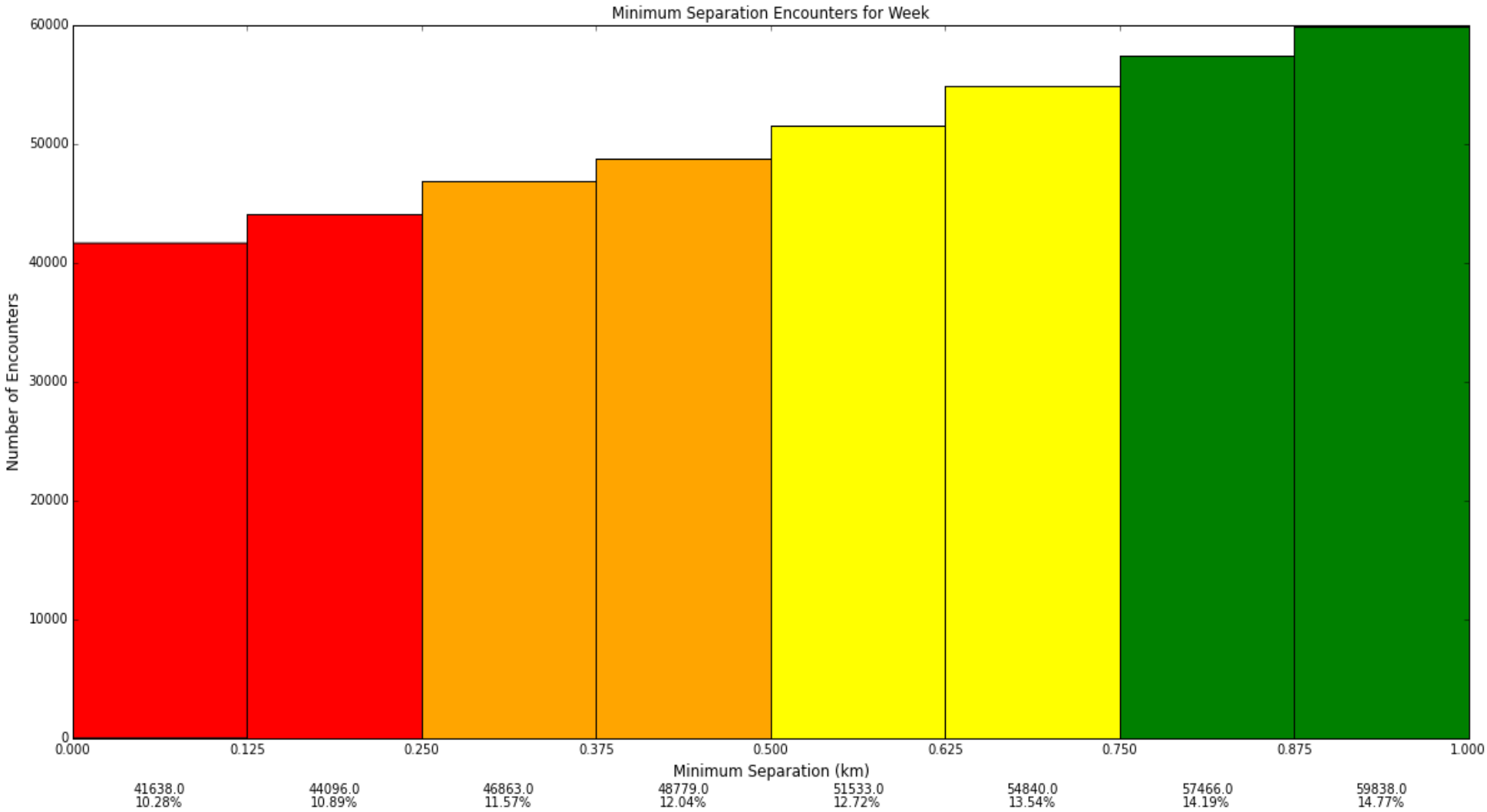

Figure 29. Histogram of minimum separation encounters for analysis week

Probability Results

The final section of this chapter will discuss the likelihood of collision results from the research. This will begin with a top-level discussion of the statistics for each collision likelihood model and conclude with some key points.

Top-Level Statistics

Table 7. Top-level statistics for the different likelihood models

	Chan	Alfano	Patera	Max
μ (weighted)	3.96E-07	3.96E-07	3.96E-07	2.16E-06
σ (weighted)	4.94E-09	4.94E-09	4.94E-09	4.06E-07
Maximum	1.00E-06	1.00E-06	1.00E-06	5.35E-02
Minimum	1.05E-07	1.05E-07	1.05E-07	1.64E-07
Chance of at Least 1 Collision (Average Daily)	4.100%	4.100%	4.100%	22.332%
Chance of at Least 1 Collision (Average Weekly)	25.699%	25.548%	25.389%	62.817%

Table 7 above presents top-level statistics for the various likelihood models used in this research. The first thing to note is the extremely small difference between the models. These models are all different approaches to the same equation and thus differ only slightly in final calculations. In fact, the average difference between the results of the first three models is only 5.1E-07.

Assuming independence of all events, the daily chance of at least one collision was calculated using the inclusion-exclusion principle defined by Equation 31 below where n is the amount of close approach events for the day.

$$\mathbb{P}\left(\bigcup_{i=1}^{n} A_i\right) = \sum_{i=1}^{n} \mathbb{P}(A_i) - \sum_{i<j} \mathbb{P}(A_i \cap A_j) \quad + \sum_{i<j<k} \mathbb{P}(A_i \cap A_j \cap A_k) - \cdots + (-1)^{n-1} \mathbb{P}\left(\bigcap_{i=1}^{n} A_i\right) \quad [31]$$

The data for this research is unique in that the individual probability of collision is so low (on the order of 10E-07). This causes the values of the equation above to come out on the order of

10E-02 10E-07 10E-15

$$\mathbb{P}\left(\bigcup_{i=1}^{n} A_i\right) = \sum_{i=1}^{n} \mathbb{P}(A_i) - \sum_{i<j} \mathbb{P}(A_i \cap A_j) \quad + \sum_{i<j<k} \mathbb{P}(A_i \cap A_j \cap A_k) - \cdots + (-1)^{n-1} \mathbb{P}\left(\bigcap_{i=1}^{n} A_i\right) \quad [32]$$

This means that the daily chance of collision is essentially dominated by the first term, leading to an approximation of the daily chance of collision being defined by

$$\mathbb{P}\left(\bigcup_{i=1}^{n} A_i\right) = \sum_{i=1}^{n} \mathbb{P}(A_i) \quad [33]$$

Furthermore, once these values have been calculated for each day of the week, they can be rolled up into a weekly chance of at least one collision using Equation 31. Since the values are on the order of 10E-02 now, the full inclusion-exclusion must be conducted. This is much more reasonable with seven values as opposed to the 700,000 needed to get the daily probability. This weekly chance of collision is shown in the final line of the table. The diameters were pulled from a linearly spaced vector spanning three millimeters to one meter with one-millimeter increments. This lead to a total of 997 possible diameters that were pulled randomly. This approach could be greatly improved by adding weights to different diameters. In its current state, there is an essentially

equally likely chance of this collision being with a three-millimeter piece as with a one-meter piece. Realistically however, the diameter measures would be heavily-skewed towards the smaller end of the spectrum. Although a three-millimeter piece is certainly preferred over a one-meter piece, it is still important to understand that a piece of that size still carries similar energy to that of a bullet. A bullet in the right location of the satellite would not be enough to cause fragmentation, but it could cause subsystem degradation or failure.

4.5 Summary

This chapter presented the results for the research. Section 4.2 was a presentation of the results for the characterization of the debris field. Section 4.3 described the features of the debris field. This included the physical characteristics, the nodal precession, and an estimated time to decay for the field. The combination of results from section 4.2 and 4.3 were used to show that Research Objective #1 had been satisfied. Section 4.4 discussed the results of the close approach analysis. The results from this analysis proved that Objective #2 had been satisfied. The time to return results after execution had begun was 105 minutes. This did not satisfy Objective #3, but this will be discussed further in Chapter 5.

V. Conclusion and Recommendations

5.1 Chapter Overview

This chapter will provide the key takeaways from the results and provide recommendations for improvement and further work on this topic. Section 5.2 presents a review of the research objectives. Section 5.3 presents the answers to the research questions. Section 5.4 provides recommendations based on the results of the research. The chapter closes out in section 5.5 with conclusions and a discussion of future work.

5.2 Review of Research Objectives

Space debris is a concerning issue for all those who operate in space, especially the Department of Defense. With the combat edge that space affords, it is imperative to be aware of the situation there at all times. Part of that awareness is being prepared to respond to emergent situations. One such event is a sudden unexpected breakup, which poses a serious threat to space-borne systems. The unpredictable nature of these events necessitates the need for Space Situational Responsiveness (SSR), or preemptive SSA. The purpose of this research was to take first steps towards defining SSR. To recap, the research objectives for this research were:

- **Research Objective #1:** Model a large-scale (100,000 pieces) debris field, propagated for one week, utilizing parallel computing on the supercomputer.
- **Research Objective #2:** Perform a close-approach analysis using the ACAT to report the number of close approaches, minimum range and separation, and likelihood of collision of the generated debris with the current catalog of on-orbit objects over the course of one week.

- **Research Objective #3:** Perform all the above and provide results within 90 minutes.

Objective #1

The primary target of this research was to use the supercomputer to model a large-scale on orbit breakup. The supercomputer was utilized as it reduced much of the computational burden by distributing the 100,000-piece breakup scenario into 500 parallel, 200-piece scenarios. This method reduced the real time to run the scenario to under two hours. While the real time is important, the true utility of the supercomputer can be seen in the computational cost. The scheme for this research utilized 250 compute nodes, each containing 36 CPUs, leading to a grand total of ~85 days of computational time needed to complete all 500 scenarios. Based on the above, objective #1 was clearly achieved.

Objective #2

In addition to modeling the debris field, the next step was to understand the dangers that such a field would impose on the space environment. STK contains the ACAT module that was perfect for such a challenge. The ACAT opened the door to running a close approach analysis on the debris pieces with the current on-orbit catalog. This allowed for a quantification of risk to be performed by demonstrating the number of close approaches and probability of collision over the course of the week. By reporting the number of close approaches, minimum range and separation, and probability of collision, the relative risk of a substantial breakup was quantified, satisfying objective #2.

Objective #3

The final objective was chosen to constrain the timeline. If this type of calculation cannot be performed quickly, then it will not be of much use in an actual scenario. This drove the final objective, which is to perform objectives one and two on an operational timeline. The operational timeline to meet was set at the average period of one LEO satellite (90 minutes). Results returned within one orbit would allow for decision-makers to have some information to work off of for potential collision avoidance maneuvers. Results for the 500-scenario scheme returned at just about 105 minutes. While this did not meet the objective, results would still be returned within two orbits. Section 5.3 will discuss some possible ways to reduce this time to meet the objective time.

5.3 Research Question Answers

At the beginning of this thesis, several research questions were posed. These questions, if answered, would satisfy the research objectives above. These questions were:

- **Research Question #1:** How can massively-parallel computation on the supercomputer be used to model large-scale debris events in STK?
- **Research Question #2:** How can the risk involved with the aforementioned debris event be quantified using STK's ACAT?
- **Research Question #3:** How can the computation time be reduced to meet an operational timeline?

Question #1

This results for the debris field compared with the FY-1C results prove that the debris field created matches historical trends. Parallelization was used to simulate 500 parallel STK scenarios with 200 debris objects in each scenario. This allowed for the simulation of a 100,000-piece debris field to be simulated in under two hours.

Question #2

The risk for the 100,000-piece event was evaluated using STK's ACAT. This tool allowed for an analysis of all close approaches with threat spheres around all objects set at one kilometer in all directions. The close approaches were characterized by minimum range, minimum separation, and likelihood of collision. The likelihood of collision was calculated using three different models to observe differences. The difference between the three models chosen for this research was found to be on the order of 10E-07. The average chance of at least one collision daily for this particular debris field was found to be 4.1% for all standard models and 22.3% for the max likelihood model. The average weekly chance of at least one collision was found to be around 25% for all standard models and 62.8% for the max likelihood model.

Question #3

The answer to Question #1 provides the bulk of the answer to Question #3. Parallelization reduced the computation time from days to about 105 minutes. As stated previously, more could be done to reduce this time. The biggest time-saver would likely be to further parallelize to 1,000 parallel, 100-piece scenarios. This would require 500 nodes on *Thunder* and would likely require a longer wait before execution. An estimate

puts the time to return results at around 70 minutes for this scheme. Another avenue to explore would be increasing the number of processes per node. The current scheme utilized an average of 3 GB of memory per run. This was nowhere near the amount of memory allocated for each process. Increasing the number of processes to 12 would reduce the amount of RAM available for each process, but allow for much faster return on results.

Another time-saver could be to reduce the number of ACATs. In early testing, reducing the number of ACATs from one per day down to just one for the whole week reduced the computational time by about 15%. This would likely drop the time into the desired operational time of 90 minutes but at the tradeoff of less positional accuracy of the propagated TLE data after the first few days. A potential middle-ground could be to run an ACAT every other day of the week to maintain positional accuracy with less computational burden.

The remaining strategies are listed below and would likely make small adjustments to the computation strategies.

- Run ACAT against a LEO-only TLE file
    - Less satellites to cross-reference debris with
- Create a report style that only includes needed information
    - COE reports give more information than needed
    - Would cut report amount in half

5.4 Recommendations

Based on the results from Chapter 4 and the discussion above, it is my recommendation that this research be continued to the next step of the operations plan, the prescribed action. This action would be the procedure undertaken to reduce the chance of collision to a desired probability. The data from this research could be utilized to import the debris field and then study an optimization of maneuvers to achieve a desired chance of collision. This research could also be more efficient as described by section 5.3 above. Additionally, due to the minor differences between the three likelihood models, it is recommended that one model be chosen and utilized. The values are so close together that any of the three could be chosen. Chan's method, being an analytical approximation, would likely be quicker than the other two numerical models. Finally. the maximum likelihood model is perhaps better suited for a single event analysis like Iridium/Cosmos, but may give overly pessimistic results for a large-scale event like this research.

5.5 Conclusion and Future Work

In conclusion, a large-scale debris field was simulated using massively-parallelized python scripting of STK on the high-performance computer, *Thunder*. This was proven successful by comparing the Gabbard plot of the field to that of the FY-1C breakup. The field was then analyzed for close approaches with the catalog of on-orbit objects using three different popular methods (Chan, Alfano, Patera, and Alfano Max). This analysis revealed over 700,000 close approaches within three kilometers over the course of one week. The daily chance of at least one collision was found to be 4.1%

across, with the weekly chance being ~25% for all standard models studied. The max likelihood model produced a daily chance of one collision of 22.3% and a weekly chance of one collision at 62.8%. Finally, the results for this simulation were returned in 105 minutes. This took longer than the desired time of 90 minutes, but recommendations were provided that would likely bring this time down well below the desired level.

Future Work

This research was posed to take a first step towards an operations plan for responding to an on-orbit breakup. After satisfying the above objectives, the first step has successfully been taken. The next step would logically be the response to such an event. Before taking this next step, the diameter distribution should be corrected to account for the distribution of the sizes of pieces. This would allow insight into not only the number of close approaches, but also the sizes of the objects involved in the close approaches. This would better define the 4.1% chance of collision by also giving the percentage chance of this collision being with a larger piece or smaller piece.

Following the diameter updates, a worthwhile endeavor would be to add an optimization of maneuvers to respond to the breakup. This could possibly be accomplished through constrained optimization. A potential method could be minimizing the Δv subject to ensuring probability of collision is below a set threshold. Additional options could be including a penalty for exceeding a certain change in altitude or inclination. These would ideally result in a maneuver that minimizes the fuel required to meet a certain probability of collision, while also remaining within an acceptable distance from the standard operational regime. Additionally, section 5.3 provided some

suggestions to reduce the computational time to the desired operational level of 90 minutes. This would allow for data return within one orbit of a typical LEO satellite, thus satisfying objective #3.

Appendix A: Supplemental Charts

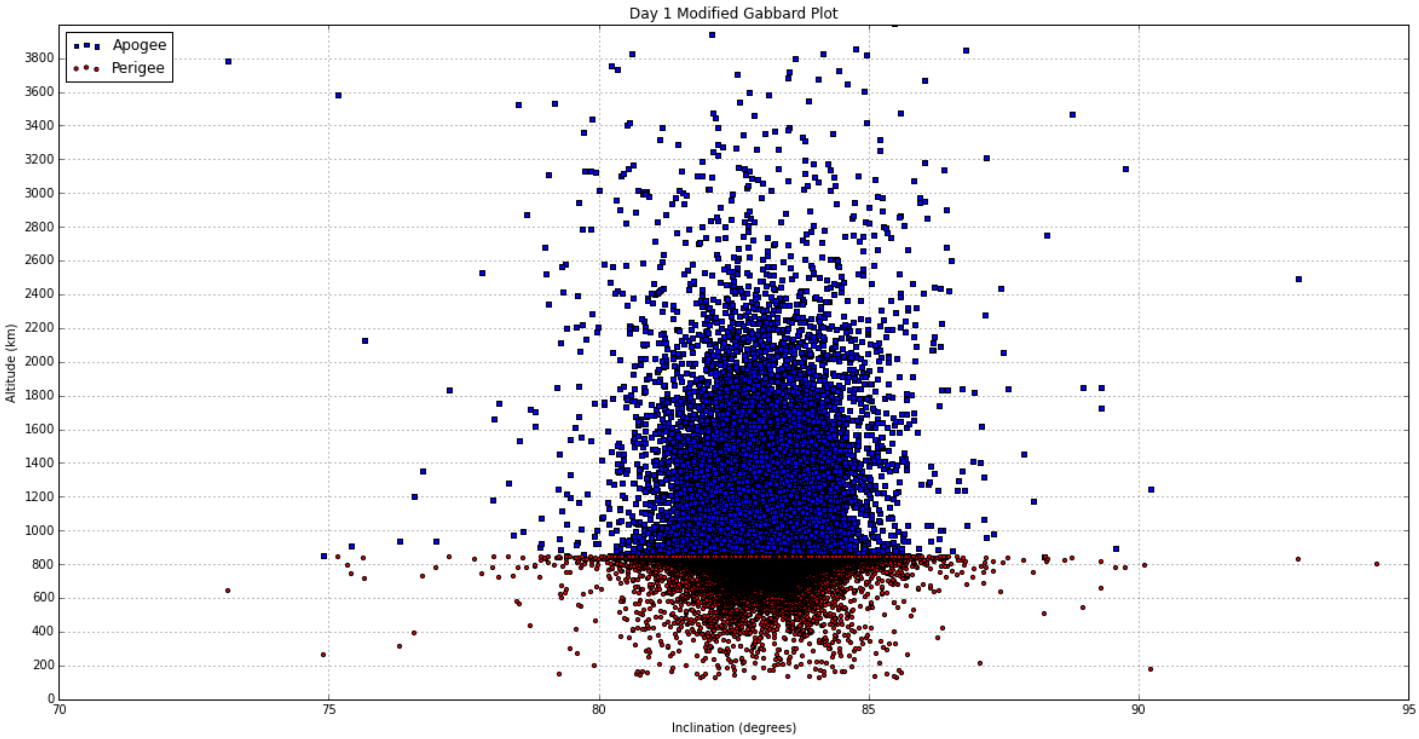

Figure 30. Day 1 constrained modified Gabbard plot

Appendix B: SGI ICE X (Thunder) System Specifications

This appendix provides a more in-depth look at the *Thunder* supercomputer from the AFRL DSRC [48]. Table 8 below provide information on all aspects of *Thunder*.

Table 8. Thunder Specification Charts

Node Configuration					
	Login Nodes	Compute Nodes			
		Standard Memory	Large Memory	GPU Accelerated	Phi Accelerated
Total Nodes	16	3,216	4	178	178
Operating System	SLES 11				
Cores/Node	28	36		28 + 2 GPU (2 x 2,880 GPU cores)	28 + 2 Phi (2 x 61 Phi cores)
Core Type	Intel E5-2699v3			Intel E5-2697v3 +NVIDIA Tesla K40M	Intel E5-2697v3 +Intel 7120P
Core Speed	2.3 GHz			2.6 GHz	
Memory/Node	128 GBytes		768 GBytes	128 GBytes +24 GBytes	128 GBytes +16 GBytes
Accessible Memory/Node	126 GBytes		766 GBytes	126 GBytes	126 GBytes +15.5 GBytes
Memory Model	Shared on node.	Shared on node. Distributed across cluster.			
Interconnect Type	4x FDR InfiniBand	4x FDR InfiniBand; Enhanced LX Hypercube			

File Systems on Thunder		
Path	Capacity	Type
/home ($HOME)	228 TBytes	Lustre
/workspace ($WORKDIR)	17.3 PBytes	Lustre

Appendix C: Creating Custom Report Styles in STK

This appendix serves as a guide for users to create new custom report styles within STK. These styles can then be uploaded to the supercomputer and created via connect commands sent to STK. It will be presented in a 2-step process. Step 1 is to create the report style within STK. Step 2 is to utilize Filezilla to place the report into the proper supercomputer directory.

Step 1: Create the report style in STK

In the STK GUI, the user will need to input an object that reports are desired for. This could be a satellite, vehicle, sensor, etc. Once this is done, navigate to the report and graph manager highlighted in Figure 31 below.

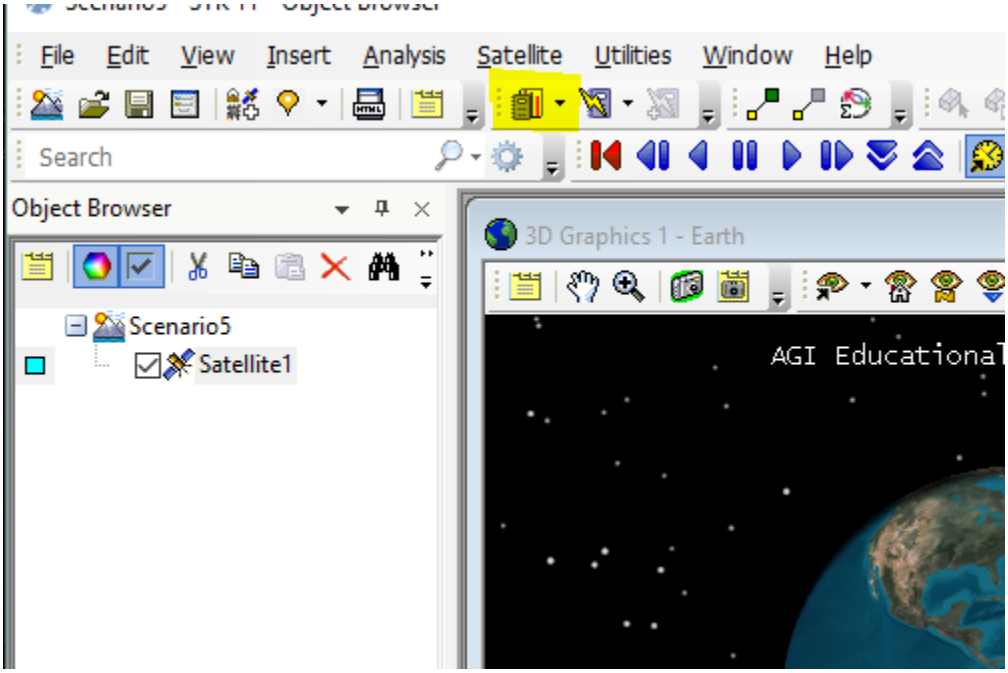

Figure 31. Locating the report and graph manager

Next, the user will need to create a new report by selecting the highlighted item in Figure 32 below.

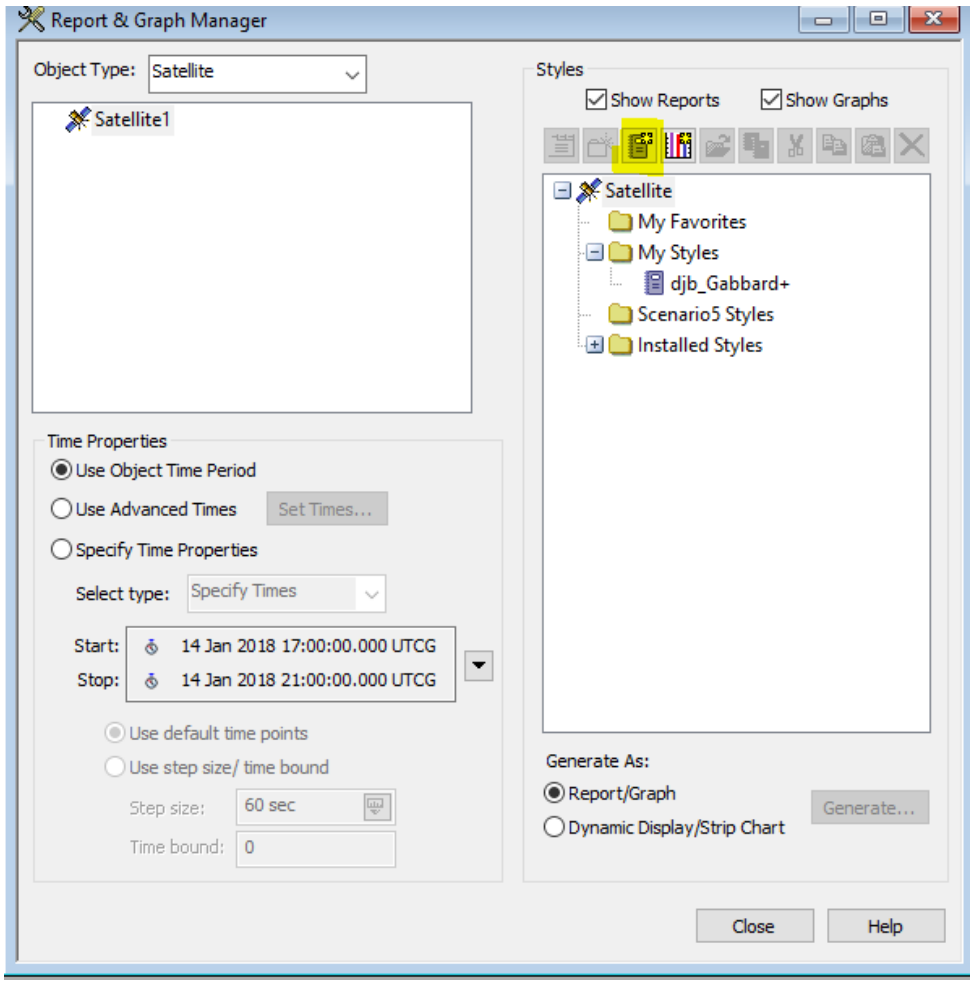

Figure 32. Locating the create new report style icon

The user will then give the report a name and define the data providers that will be included in the report. Full details on data providers can be found at the following link: http://help.agi.com/stk/Subsystems/dataProviders/dataProviders.htm. After adding the appropriate lines to the report, the user will click apply and the report will be saved to the STK Config directory, leading to step 2.

Step 2: Utilize FileZilla to place the .rst file into the proper directory

This step will require the user to open FileZilla. Once FileZilla is open, use the left half of the application (the home computer side) to navigate down the following path:

C:/Users/[user name]/Documents/STK 11 (x64)/Config/Styles

Once in the Styles folder, select the object folder that the custom report was created for (it should be the only available object if this is the first custom report made). The .rst file will be in the folder.

Once in the proper folder on the left side, the next step is to open the appropriate destination folder on the right side (the supercomputer side). The proper directory path for the supercomputer is as follows:

/p/home/[user name]/stk11.x.0/STKData/Styles

Once in styles, use the same process as above and open the appropriate object directory. The final step is to simply drag the .rst file from the left side of the application into the directory on the right side. From now on the user can call their custom report by name using the ReportCreate connect command.

Bibliography

[1] M. Wall, “Space.com Envisat Article May 2012,” *Space*, 2012. [Online]. Available: http://www.space.com/15640-envisat-satellite-space-junk-150years.html. [Accessed: 29-May-2017].

[2] R. Thompson, “Aero Corp Space Debris Primer,” *Crosslink*, Dec-2015. [Online]. Available: http://www.aerospace.org/crosslinkmag/fall-2015/a-space-debris-primer/.

[3] European Space Agency, “Space Debris by the Numbers,” *European Space Agency*, 2017. [Online]. Available: http://www.esa.int/Our_Activities/Operations/Space_Debris/Space_debris_by_the_numbers. [Accessed: 17-Jan-2018].

[4] J. Yoder, “Stuff in Space,” 2018. [Online]. Available: http://stuffin.space/. [Accessed: 03-Jan-2018].

[5] U.S. Joint Chiefs of Staff, “Space Operations,” *Jt. Publ. 3-14*, no. May, 2013.

[6] M. Sheetz, “The space industry will be worth nearly $3 trillion in 30 years, Bank of America predictsThe space industry will be worth nearly $3 trillion in 30 years, Bank of America predicts,” *CNBC*, 2017. [Online]. Available: https://www.cnbc.com/2017/10/31/the-space-industry-will-be-worth-nearly-3-trillion-in-30-years-bank-of-america-predicts.html. [Accessed: 27-Nov-2017].

[7] Aerospace Corporation, “Understanding Space Debris,” *Crosslink*, vol. 16, no. 1, pp. 1–61, 2015.

[8] T. Carrico, J. Carrico, L. Policastri, and M. Loucks, “Investigating orbital debris events using numerical methods with full force model orbit propagation,” *Adv. Astronaut. Sci.*, vol. 130 PART 1, pp. 407–426, 2008.

[9] M. La Vone, “Kessler Syndrome,” *Space Safety Magazine*. [Online]. Available: http://www.spacesafetymagazine.com/space-debris/kessler-syndrome/. [Accessed: 22-Aug-2017].

[10] J. W. Wagner, “Beware the situation: how JSpOC tracks space debris,” *Room Sp. J.*, vol. 1, no. 1, 2014.

[11] J. C. Liou, “USA Space Debris Environment, Operations, and Policy Updates,” in *54th Session of the Scientific and Technical Subcommittee*, 2017, pp. 1–14.

[12] National Research Council, *Orbital Debris A Technical Assesment*. Washington, DC: National Academy Press, 1995.

[13] United Nations Office for Outer Space Affairs, “Space Debris Mitigation Guidelines of the Committee on the Peaceful Uses of Outer Space,” *United Nations Publ.*, p. 12, 2010.

[14] Joint Space Operations Center, “Space-Track Box Score,” *Space-Track*, 2017. [Online]. Available: https://www.space-track.org/#/boxscore. [Accessed: 07-Aug-2017].

[15] European Space Agency, “Copernicus Sentinel-1A Satellite Hit By Space Particle,” *ESA*, 2016. [Online]. Available: http://www.altestore.com/store/Solar-Panels/51-to-99-Watt-Solar-Panels/BP-Solar-585U-85W-12V-Solar-Panel/p2708/. [Accessed: 08-Aug-2017].

[16] M. Gruss, “Haney: U.S. Partners To Have Indirect Access to Space Fence Data,” *Space News*, 2014. [Online]. Available: http://spacenews.com/42619haney-us-partners-to-have-indirect-access-to-space-fence-data/. [Accessed: 27-Nov-2017].
[17] A. Rossi, A. Cordelli, P. Farinella, L. Anselmo, and C. Pardini, “Long term evolution of the space debris population,” *Adv. Sp. Res.*, vol. 19, no. 2, pp. 331–340, 1997.
[18] European Space Agency, “IMPACT CHIP,” *European Space Agency*, 2016. [Online]. Available: http://www.esa.int/spaceinimages/Images/2016/05/Impact_chip. [Accessed: 07-Aug-2017].
[19] D. S. F. Portree and J. P. Loftus, “Orbital Debris: A Chronology (NASA/TP-1999-208856),” no. January, p. xii+158, 1999.
[20] NASA, “Orbital Debris Quarterly News July 2010,” *Orbital Debris Q. News*, vol. 14, no. 3, pp. 1–12, 2010.
[21] E. Vitt, “Space debris. Physical and legal considerations,” *Space Policy*, vol. 5, no. 2, pp. 129–137, 1989.
[22] NASA, “Guidelines and Assessment Procedures for Limiting Orbital Debris,” *NASA Saf. Stand.*, vol. 1740, no. 14, 1995.
[23] Office of the President of the United States, “National Space Policy of the United States of America,” *Exec. Off. Pres.*, p. 18, 2010.
[24] E. Howell, “Space Junk Cleanup,” *Space*, 2014. [Online]. Available: https://www.space.com/24895-space-junk-wild-clean-up-concepts.html. [Accessed: 11-Aug-2017].
[25] D. J. Kessler and B. G. Cour-Palais, “Collision Frequency of Artificial Satellites: The Creation of a Debris Belt,” *J. Geophys. Res.*, vol. 83, no. 8, pp. 918–924, 1978.
[26] T. S. Kelso, “SATCAT Growth,” *CelesTrak*, 2017. [Online]. Available: http://www.celestrak.com/satcat/growth.png. [Accessed: 10-Aug-2017].
[27] T. S. Kelso, “Analysis of the 2007 Chinese ASAT Test and the Impact of its Debris on the Space Environment,” *Adv. Maui Opt. Sp. Surveill. Technol.*, pp. 321–330, 2007.
[28] W. Wiesel, *Spaceflight Dynamics*, 3rd ed. Beavercreek: Aphelion Press, 2010.
[29] NASA, “Orbital Debris Quarterly News April 2007,” *Orbital Debris Q. News*, vol. 11, no. 2, pp. 1–10, 2007.
[30] NASA, “Orbital Debris Quarterly News July 2007,” *Orbital Debris Q. News*, vol. 11, no. 3, pp. 1–10, 2007.
[31] NASA, “Orbital Debris Quarterly News January 2009,” *Orbital Debris Q. News*, vol. 13, no. 1, pp. 1–12, 2009.
[32] M. McKinnon, ““ History of Garbage ”,” *Gizmodo*, 2014. [Online]. Available: http://gizmodo.com/a-history-of-garbage-in-space-1572783046. [Accessed: 15-Aug-2017].
[33] US Government, “U.S. Government Orbital Debris Mitigation Standard Practices,” pp. 1–4.
[34] L. Hutchinson, “How NASA steers the International Space Station around space

junk," *Ars Technica*, 2013. [Online]. Available: https://arstechnica.com/science/2013/07/how-nasa-steers-the-international-space-station-around-space-junk/. [Accessed: 15-Aug-2017].
[35] NASA, "The Day NASA's Fermi Dodged a 1.5-ton Bullet," *Fermi Mission Page*, 2013. [Online]. Available: https://www.nasa.gov/mission_pages/GLAST/news/bullet-dodge.html. [Accessed: 15-Aug-2017].
[36] T. S. Kelso, "CelesTrak - More Frequently Asked Questions," *Satellite*, 2014. [Online]. Available: http://www.celestrak.com/columns/v04n05/. [Accessed: 07-Jan-2018].
[37] F. R. Hoots and R. L. Roehrich, "Spacetrack Report No. 3--Models for Propagation of NORAD Elements Sets," *Spacetrack Rep.*, vol. 3, no. 3, pp. 1–91, 1980.
[38] W. Dong and Z. Chang-yin, "An Accuracy Analysis of the SGP4/SDP4 Model," *Chinese Astron. Astrophys.*, vol. 34, no. 1, pp. 69–76, 2010.
[39] S. Alfano, "Review of conjunction probability methods for short-term encounters," *Adv. Astronaut. Sci.*, vol. 127 PART 1, pp. 719–746, 2007.
[40] K. Chan, "Short-Term vs Long-Term Spacecraft Encounters," *AIAA Pap.*, no. August, pp. 1–21, 2004.
[41] R. P. Patera, "A general method for calculating satellite collision probability," *Adv. Astronaut. Sci.*, vol. 105 II, no. 4, pp. 1275–1290, 2000.
[42] S. Alfano, "Relating position uncertainty to maximum conjunction probability," *J. Astronaut. Sci.*, vol. 53, no. 2, pp. 193–205, 2005.
[43] T. S. Kelso and S. Alfano, "Satellite Orbital Conjunction Reports Assessing Threatening Encounters in Space (SOCRATES)," *Eur. Sp. Agency, (Special Publ. ESA SP*, no. 587, pp. 737–740, 2005.
[44] S. Alfano, "Addressing Nonlinear Relative Motion For Spacecraft Collision Probability," *Am. Inst. Aeronaut. Astronaut.*, pp. 1–10, 2006.
[45] J. C. . J. N. L. . K. P. H. . A.-M. P. D. Liou, "The new NASA orbital debris breakup model," *COSPAR Colloq. Ser.*, vol. 15, pp. 363–367, 2002.
[46] H. Klinkrad, "Space Debris Models and Risk Analysis," in *Space Debris Models and Risk Analysis*, Chichester, 2006, pp. 67–76.
[47] N. L. Johnson, P. H. Krisko, J. C. Liou, and P. D. Anz-Meador, "NASA's new breakup model of EVOLVE 4.0," *Adv. Sp. Res.*, vol. 28, no. 9, pp. 1377–1384, 2001.
[48] AFRL DSRC, "SGI Ice X (Thunder) User Guide," *AFRL DSRC*. [Online]. Available: https://www.afrl.hpc.mil/docs/thunderUserGuide.html#intro. [Accessed: 14-Jan-2018].
[49] M. Matney, "Gabbard Plot Discussion," *NASA Tech. Rep.*, pp. 0–7, 2017.
[50] JSPOC, "Space-Track Bulk Catalog Download," *Space-Track*, 2018. [Online]. Available: https://www.space-track.org/#/recent. [Accessed: 27-Jan-2018].
[51] T. S. Kelso, "CelesTrak Iridium Cosmos," *CelesTrak*, 2012. [Online]. Available: http://celestrak.com/events/collision/. [Accessed: 29-May-2017].

SF-298

REPORT DOCUMENTATION PAGE

Form Approved
OMB No. 074-0188

PLEASE DO NOT RETURN YOUR FORM TO THE ABOVE ADDRESS.

1. REPORT DATE *(DD-MM-YYYY)*	2. REPORT TYPE	3. DATES COVERED *(From – To)*
23-03-2018	Master's Thesis	August 2016 – March 2018

TITLE AND SUBTITLE

Utilizing Supercomputing to Analyze Risks of An Emergent Large-Scale Debris Field in Low Earth Orbit

5a. CONTRACT NUMBER

5b. GRANT NUMBER

5c. PROGRAM ELEMENT NUMBER

6. AUTHOR(S)

Buehler, David J., Second Lieutenant, USAF

5d. PROJECT NUMBER

5e. TASK NUMBER

5f. WORK UNIT NUMBER

7. PERFORMING ORGANIZATION NAMES(S) AND ADDRESS(S)

Air Force Institute of Technology
Graduate School of Engineering and Management (AFIT/EN)
2950 Hobson Way, Building 640
WPAFB OH 45433-8865

8. PERFORMING ORGANIZATION REPORT NUMBER

AFIT-ENV-MS-18-M-184

9. SPONSORING/MONITORING AGENCY NAME(S) AND ADDRESS(ES)

Undisclosed

10. SPONSOR/MONITOR'S ACRONYM(S)

11. SPONSOR/MONITOR'S REPORT NUMBER(S)

12. DISTRIBUTION/AVAILABILITY STATEMENT

DISTRUBTION STATEMENT A. APPROVED FOR PUBLIC RELEASE; DISTRIBUTION UNLIMITED.

13. SUPPLEMENTARY NOTES

14. ABSTRACT

The likelihood of on-orbit breakups, whether spontaneous or the result of collision, will likely continue to grow as the barriers of entry to and use of space are reduced. In all orbital regimes, especially low Earth orbit (LEO), preparation to respond quickly when the next breakup occurs is critical. This research utilizes high-performance parallel computation along with python-driven Systems Tool Kit (STK) to model a large-scale on-orbit breakup in LEO, with the goal of returning data in less than 90 minutes. The breakup is characterized by the National Aeronautics and Space Administration (NASA) EVOLVE 4.0 breakup model and is both dialable and scalable.

The debris field is analyzed over the course of one week using Gabbard plots. The risk posed by the breakup is determined using STK's Advanced Close Approach Tool (ACAT) to report minimum range, minimum separation, and likelihood of collision between the debris and catalog. The field is screened for close approaches each day of the week and the probability of collision is computed using multiple conjunction models (Alfano, Patera, Chan, Alfano Max) to observe how different models predict the likelihood of collision. The goal is to take steps towards preparing to respond to breakup events in the future.

15. SUBJECT TERMS

Space Debris

16. SECURITY CLASSIFICATION OF:			17. LIMITATION OF ABSTRACT	18. NUMBER OF PAGES	19a. NAME OF RESPONSIBLE PERSON
a. REPORT	b. ABSTRACT	c. THIS PAGE			Col. Dane Fuller, AFIT/ENY
U	U	U	UU	99	19b. TELEPHONE NUMBER *(Include area code)* (937) 255-3636, ext 4679 (dane.fuller@afit.edu)

Standard Form 298 (Rev. 8-98)
Prescribed by ANSI Std. Z39-18